U.S. Army Research Institute of Environmental Medicine

Natick, Massachusetts

TECHNICAL NOTE NO. T24-008
DATE: May 2024
AD

METHODOLOGICAL CONSIDERATIONS IN MODELING OF BIOMECHANICS OF PARACHUTE OPENING SHOCK

United States Army
Medical Research & Development Command

USARIEM TECHNICAL REPORT T24-008

METHODOLOGICAL CONSIDERATIONS IN MODELING OF BIOMECHANICS OF PARACHUTE OPENING SHOCK

Juan Baus[1]

William J. Tharion[2]

James Yang[1]

[1]Texas Tech University, Lubbock, TX

[2]U.S. Army Research Institute of Environmental Medicine (USARIEM), Natick, MA

May 2024

U.S. Army Research Institute of Environmental Medicine

Natick, MA 01760-5007

REPORT DOCUMENTATION PAGE

Form Approved
OMB No. 0704-0188

1. REPORT DATE *(DD-MM-YYYY)*	2. REPORT TYPE	3. DATES COVERED *(From - To)*
15-05-2024	Technical Report	2022-2024

4. TITLE AND SUBTITLE

METHODOLOGICAL CONSIDERATIONS IN MODELING OF BIOMECHANICS OF PARACHUTE OPENING SHOCK

5a. CONTRACT NUMBER

W81XWH-15-9-0001

5b. GRANT NUMBER

5c. PROGRAM ELEMENT NUMBER

6. AUTHOR(S)

Juan Baus, William J. Tharion, JamesYang

5d. PROJECT NUMBER

MO210316_IE

5e. TASK NUMBER

5f. WORK UNIT NUMBER

7. PERFORMING ORGANIZATION NAME(S) AND ADDRESS(ES)

Texas Tech University, Lubbock, TX, 79409

Military Performance Division, U.S. Army Research Institute of Environmental Medicine. Building 42 - 10 General Greene Ave, Natick, MA 01760

8. PERFORMING ORGANIZATION REPORT NUMBER

T24-008

9. SPONSORING/MONITORING AGENCY NAME(S) AND ADDRESS(ES)

U.S. Army Medical Research and Development Command,
Fort Detrick, MD 21702

10. SPONSOR/MONITOR'S ACRONYM(S)

11. SPONSOR/MONITOR'S REPORT NUMBER(S)

12. DISTRIBUTION/AVAILABILITY STATEMENT

Approved for public release; distribution unlimited

13. SUPPLEMENTARY NOTES

14. ABSTRACT

The current research project analyzed the biomechanics of military parachute operations, specifically focusing on the challenging context of free-fall jumps. Using inertial measurement units (IMUs) and validated musculoskeletal models, this study aims to understand the impact of external forces during critical phases of the jump, notably the impact of the tethered snatch (i.e., a bundle of equipment that is free from the jumper but tethered to the jumper) and parachute opening shock resulting from both the jumper's body but also the tethered bundle. The impact of this opening shock on the musculoskeletal upper body and the body's muscle activation response was explored.

15. SUBJECT TERMS

predictive modeling; simulation, parachuting; parachute opening shock, HALO, HAHO, algorithms, Special Operations Command, SOCOM, musculoskeletal injuries

16. SECURITY CLASSIFICATION OF:			17. LIMITATION OF ABSTRACT	18. NUMBER OF PAGES	19a. NAME OF RESPONSIBLE PERSON
a. REPORT	b. ABSTRACT	c. THIS PAGE			William J. Tharion
Unclassified	Unclassified	Unclassified	Unclassified	38	19b. TELEPHONE NUMBER *(Include area code)* 508-206-2400

Reset

Standard Form 298 (Rev. 8/98)
Prescribed by ANSI Std. Z39.18

DISCLAIMERS

This report's views, opinions, and/or findings are those of the author(s) and should not be construed as an official Department of the Army, Department of Defense, or U.S. Government position, policy, or decision unless designated by other official documentation. Citation of trade names in this report does not constitute an official Department of the Army, Department of Defense, or U.S. Government endorsement or approval of using such commercial items.

This research was partly supported by an appointment to the Postgraduate Research Program at the U.S. Army Aeromedical Research Laboratory administered by the Oak Ridge Institute for Science and Education through an interagency agreement between the U.S. Department of Energy and the U.S. Army Medical Research and Development Command (MRDC).

This work is for public release.

TABLE OF CONTENTS

LIST OF FIGURES

LIST OF TABLES

ACKNOWLEDGEMENTS

The authors would like to thank the following individuals for their assistance in preparing this technical report:

Thanks to all other members of the Human-Centric Design Research Laboratory (HCDRL) at Texas Tech University for their support during this project, especially in the preliminary data processing stage.

Thanks to Tyler F. Rooks and Haley A. French Krahn from the U.S. Army Aeromedical Research Laboratory (USAARL) for providing the secondary data that was used for the kinetic and kinematic analysis of the musculoskeletal models. We also acknowledge Reed Hoyt at USARIEM for obtaining funding and for providing scientific advice to the team for this research project.

Funding for the research came from the Medical Research and Development Command (MRDC) through USARIEM and the Medical Technology Enterprise Consortium (MTEC).

EXECUTIVE SUMMARY

The current research project goals are to analyze the biomechanics of military parachute operations, specifically focusing on the challenging context of free-fall jumps. Using inertial measurement units (IMUs) and validated musculoskeletal models, this study aims to understand the impact of external forces during critical phases of the jump, notably the impact of the tethered snatch (i.e., a bundle of equipment that is free from the jumper but tethered to the jumper) and parachute opening shock resulting from both the jumper's body but also the tethered bundle. The impact of this opening shock on the musculoskeletal upper body and the body's muscle activation response is explored. The investigation incorporates four distinct datasets collected by the U.S. Army Aeromedical Research Laboratory (USAARL), Fort Novosel, AL, varying in loading conditions, jump types (bundle and no-bundle), and jump altitudes (High-Altitude Low-Opening - HALO and High-Altitude High-Opening - HAHO). Seven sensors strategically placed on the jumper's body provide detailed measurements, including acceleration, magnetic field, barometric pressure, temperature, orientation, and relative and absolute time.

The methodology is divided into three parts. First, modeling and simulation based on secondary experimental data involves using two musculoskeletal models: the Dynamic Avatars with Complete Articulated Anatomy (DACAA) of the upper body and a shoulder model (an upper body model with detailed definition around the shoulder joint). Model calibration includes scaling and IMU placement, ensuring accurate representation in the simulation. Second, external forces, simulating tether snatch and parachute opening shock, are applied based on accelerometer data, allowing for a detailed analysis of the musculoskeletal upper body response. Finally, the study explores muscle activation prediction to understand body response behavior under extreme loading conditions.

BACKGROUND

This study investigates previously unexplored facets of military parachute operations, specifically focusing on tandem bundle operations. One factor that stands out in this study is combining sensor measurements during parachute openings with various modeling techniques to examine how parachute jumpers' bodies react to different loading conditions. The United States Special Operations Command (SOCOM) tactically uses the technique of tethering loads they will use on the ground to the jumper to ensure the equipment needed on the ground arrives in the same location as the jumper. The decision to focus on tandem jumps (i.e., where the jumper and the equipment bundle are in tandem) is because, in this parachute jumping technique, the jumpers use a larger parachute capable of carrying heavy weight. This same reason leads to an increased injury risk due to the heavy tandem tethered bundles that jumpers need to carry along their gear. Previous research projects have concentrated on static line operations due to the nature of the jump, where the parachute is deployed automatically without the jumpers' intervention. In this study, the analysis is concentrated on different scenarios of free-fall jumps where the jumper is responsible for pulling the rip cord to open the parachute.

The wide body of literature takes a physics-orientated approach to understanding parachute mechanics in different conditions, but it lacks information on how those mechanics affect the jumper. Anecdotal reports from trained jumpers suggest potential health hazards during the free-fall and tethered tandem bundle operations. Instead of focusing on the physics of the parachute, the goal was to improve the understanding of whether the current military equipment allows jumpers to carry heavy bundles safely. The selected approach could analyze the response of various musculoskeletal models during various instances during the task, like aircraft exit, tether snatch, and parachute opening shock. Ultimately, this study aims to enhance the safety and effectiveness of these operations for SOCOM jumpers and directly relates to the health and performance of these SOCOM jumpers during these specialized military operations.

INTRODUCTION

There are many airborne operations that the U.S. Army uses to deploy soldiers into combat areas. The most common and well-documented technique is the static line parachute jump, where the jumper does not need to act for parachute deployment. The occurrences of injury in this type of jumping are reported in the literature, and it depends on factors like equipment carried, wind speed, aircraft type, and terrain type, among other variables (1–3). On the other hand, military free-fall jumps require precise control of the parachute for its opening and steering. Military free-fall jumps are even more challenging when military personnel carry heavy loads on or tethered to their body (i.e., tandem free-fall jumps or tandem bundle free-fall jumps). In some cases, the jumps are from a higher altitude than the previous case (static line parachute jump), causing different potential risk factors (4–6). Depending on the jumper's altitude when leaving the plane and the parachute opening altitude, there are two types of free-fall jumps defined in the FM 3-05.211, Special Forces Military Free-Fall Operations (7):

> High-Altitude Low-Opening (HALO) is a jump made with an exit altitude of up to 35,000 feet above sea level and a parachute deployment altitude at or below 6,000 feet above ground level (7).
>
> High-Altitude High-Opening (HAHO) operations are standoff infiltration jumps made with an exit altitude of up to 35,000 feet above sea level and a parachute deployment altitude at or above 6,000 feet above ground level (7).

The complexity of these operations makes it challenging for experimental scientists to analyze military free-fall jumps since any modification of the jumping protocol could be expensive and, in some cases, can increase injury risk for jumpers. Musculoskeletal modeling approaches are an alternative to test and analyze parachute jumping tasks. Video-based motion capture data have traditionally driven the musculoskeletal models to obtain kinetic and kinematic responses to the human body (8). Even when previous studies have successfully proven that it is possible to feed a musculoskeletal model with experimental data to obtain joint angles, moments, and muscle activation, it is impossible to replicate the necessary laboratory environment during mid-air operations (9,10). The methodology presented in laboratory-based studies is insufficient to capture human body motion in environments where video-based motion capture is impossible. Nonetheless, the methodology presented in previous studies is worth considering in developing a novel procedure to analyze the parachute jumping task.

Optical motion capture devices have traditionally been used to track human body motion, but the need for a laboratory setup with limited workspace is a considerable constraint. A recently developed alternative to video-based motion capture data is sensor-based motion capture, which has the necessary accuracy for musculoskeletal modeling applications (11–16). Modern inertial measurement units (IMUs) have been tested in many biomechanical applications, making them suitable for tracking body

kinematics in highly dynamic scenarios (17–20); however, they have never been used in parachute operations. Sensor-based motion capture with IMUs could be a well-suited alternative for monitoring body segment orientation during parachute jumping tasks. Previous researchers have analyzed the differences between the optical and IMU-based motion capture systems and suggested that both are valid and reliable for tracking body kinematics (21). These sensors can output orientations calculated through sensor fusion of the accelerometer, gyroscope, and magnetometer data. The resulting fusion of this data is represented as unit quaternions (22). Triaxial accelerometers like those presented in IMU sensors have been combined with surface electromyography (EMG) to analyze the muscle response due to high accelerations during the parachute opening shock (23).

Helmet, body, and gear sensor packages have been proven to successfully collect kinematic data to evaluate head and torso accelerations during the parachute opening shock (24). Even when previous studies have used EMG sensors during the jumping task to study neck pain, the temporal data lacks precision when synchronized with the parachute opening shock data (25). The versatility of IMU sensors is the key point for data collection since sensor data can be obtained from accelerometers, gyroscopes, magnetometers, and barometers simultaneously. Even when muscle force and activation are not directly measured with IMUs, it may be possible to estimate them based on kinetic and kinematic data (26). Simulation and modeling approaches have been explored to overcome data collection difficulties during parachute jumping tasks. Simulation methods have been used for parachute jumping training where a skeletal model can track the jumper’s postures and extract kinematic variables like upper body joint angles (8). Most previous studies have concentrated on the parachute opening shock instant during the jumping task because of the high prevalence of neck pain among parachute jumpers (27). Parachute opening shock has been widely studied in aerodynamics, but the physics-based approach to understanding this phenomenon does not provide insight into the musculoskeletal response the jumpers’ bodies experience (28,29). The analysis of the neck response to the parachute opening shock is challenging due to the complexity of the tissues that comprise the human spine and surrounding structures. Instrumenting cadavers and dummies provide only limited conclusions (30). Addressing the musculoskeletal response to external loading is complex and requires an efficient approximation to represent the human body's interaction with parachute gear and equipment.

Biomechanical modeling and simulation techniques can offer the necessary information to understand the human body’s response during parachute jumping. Regarding kinematic analysis, the IMU sensors could animate a musculoskeletal model by recording segment orientations. Since the parachute opening shock causes loading on the body of the jumper through the harness, calculating or measuring the opening shock force is essential. Different methods have been proposed to estimate these forces, but none efficiently applies to estimating the parachute risers’ (the ropes attached to body’s harness and the parachute canopy that also allow the jumper to steer the parachute) forces during the opening shock (31,32). Although the opening shock instant

represents a high injury risk for jumpers, it is not the only period examined in this study. As mentioned above, some jumping tasks require jumpers to carry high loads, which could represent additional risk due to the external loading when leaving the aircraft (33,34). In the case of bundle jumps, the tether snatch pull is also a potential source of injury.

Work-related injury risk assessments have been done with participants using wearable devices (35). Considering that the task in this study described above is considerably different, the same methodology (use of wearable devices) cannot be followed. Since the neck may be vulnerable during the parachute opening shock due to inertial loading, voluntary muscle control is studied with various types of data like the joint motion (kinematics), the causes of that motion (kinetics), and the human body's physiological responses (dynamic joint strength, muscle force, and activation) (36). It has been reported that pain and injuries related to parachute opening shock correspond to 25% to the neck, 18% to the lower back, 16% to the shoulders, and 10% to the thoracic spine (37). This study does not examine the impact of parachute landing. Therefore, the analysis is concentrated on the area around the neck, and data is obtained to gain insight into the complete upper-body response during key periods of the jumping task. This study aims to define the principles and propose guidelines for a multiscale analysis methodology. The proposed methodology should help guide future data collection and processing for parachute jumping-related tasks. The analysis focuses on body kinetics and kinematics of the upper body in different jumping conditions, e.g., different carried loads in HALO and HAHO jumps.

METHODS

DATASETS

The methods described within this report use secondary data corresponding to four data sets, identified with color names, collected by the U.S. Army Aeromedical Research Laboratory (USAARL), Fort Novosel, AL, from the same jumper during multiple military free fall jumps, with the characteristics shown in Table 1. These datasets were selected to compare different loading conditions in bundle vs. no-bundle jumps and HALO vs. HAHO jumps. The datasets include information on seven sensors named "RightUpperArm," "RightLowerArm," "LeftUpperArm," "LeftLowerArm," "Belly," "Chest," and "Head." The available information from each sensor includes measurements of acceleration, magnetic field, barometric pressure, temperature, orientation, and relative and absolute time.

Table 1. Datasets Characteristics

	Purple	Yellow	New Yellow	Red
Type	HALO	HALO	HALO	HAHO
Bundle	Yes	No	Yes	Yes
Jumper weight	185 lb	185 lb	185 lb	185 lb
Bundle weight	423 lb	-	480 lb	650 lb
All up weight	723 lb	320 lb	780 lb	955 lb

Considering that the following analyses require the use of this information, m_1 is defined as the difference between all up weight and the bundle weight, while m_2 corresponds to the bundle weight. That is, m_1 represents the jumper's weight plus the weight of the gear the jumper carries.

MUSCULOSKELETAL MODELS SELECTION

Many different musculoskeletal models for the open-source software OpenSim® are available online (38,39). The models differ in muscle definition, number of bodies (individual bones or groups of bones that move together), and degrees of freedom per joint. The most recent version of OpenSim includes the OpenSense module with the IMU placement and inverse kinematics tools (40,41). OpenSim is an application developed by Simbios, a National Institute of Health Center for Biomedical Computation, at Stanford University and is used for biomechanical modeling, analysis and simulation. For inverse kinematics tools, storing the orientations as quaternions allows the skeletal bodies to rotate in space through the inverse kinematics calculations. It is important to mention that quaternions do not provide information for translation in space.

After testing various models, this project selected the Dynamic Avatar with Complete Articulated Anatomy (DACAA) model (42) for the upper body analysis and the neck response. The DACAA model was developed by combining multiple validated models for the lower body (43), vertebral spine (44), and upper extremities (45). One advantage of the DACAA model is that it has been updated to work in the latest OpenSim versions, including the IMU placement tools and inverse kinematics. Even when the DACAA model is a full-body model, it was modified by removing the bones, muscles, and joints corresponding to the legs and their connection to the pelvis.

The Saul model was also used (45–47) to simulate the shoulder response. Compared to the DACAA model, the Saul model has a more detailed definition of the muscles around the shoulder area. Other more detailed musculoskeletal models were not considered since their complexity was not compatible with the sensor placement protocol selected to collect the data in the simulation and modeling analysis. Any model selection does not imply that the selection is unique; there might be other valid models, and other sensor protocols that could require other specifications. Nevertheless, considering that

each research project has its own requirements, finding a model that tracks the desired variables while keeping its computational efficiency is what is necessary and that is what was done in this report's model description.

MUSCULOSKELETAL MODEL CALIBRATION

Model calibration involves the ability to scale and precise IMU placement. In this case, musculoskeletal model scaling was unnecessary since the generic model has the same height as the jumper participating in the tasks. To scale the musculoskeletal model, OpenSim offers various options. Modifying scaling factors is a simple and efficient way to scale the model to the desired anthropometrics. After scaling the musculoskeletal model, the IMU placement step is done in OpenSim by assigning each sensor to a body in the model. This assignment requires defining the IMU's rotation with respect to the global reference frame when the musculoskeletal model is in the neutral posture, meaning that all joint angles are set to zero displacement.

The following step can be executed by collecting a calibration trial where the participant stands in the same posture as the model so that each sensor orientation will be set for the calibration posture. The nature of the data used for this project did not allow us to follow that procedure. Even when data is available where the participant stands in a calibration pose, the sensor orientation was incompatible with the OpenSim requirements to run the IMU placement tool. Therefore, a different calibration approach was developed by looking at the photograph taken after the sensors were placed on the jumpers' bodies. The photographs show the location and the orientation of the sensor as seen in Figure 1. The sensor protocol used to collect data uses seven sensors placed over the head, chest, abdomen, and right and left arms and forearms. The figure also shows the local reference frame of the Opal © sensors (APDM Wearable Technologies INC., Portland, OR) (35). Consequently, the calibration was possible by knowing the sensor orientation and the manufacturer's definition of the z-axis being normal to the sensor's screen.

Figure 1. Sensor Placement and Local Reference Frame

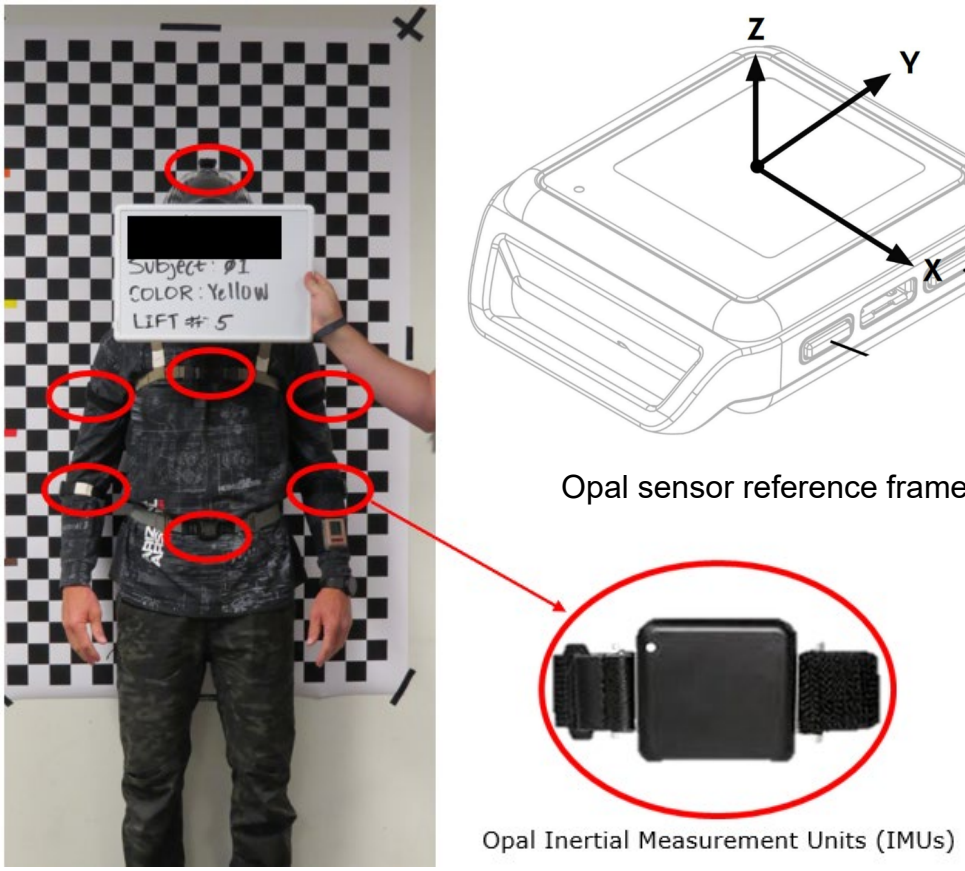

Data were collected and stored in a .h5 file at an 800 Hz data rate for approximately an hour and a half for each data set. Data were trimmed to a few minutes and down sampled to a third of the original data rate, corresponding to 267 Hz, to reduce the processing time. No pre-filtering step was done before down sampling of the data. The trimming criteria were guided by the barometric data collected with the IMUs and “event markers” created during the data collection. The “event markers” correspond to time frames when events of interest started or ended, like the jumper standing in a neutral posture for the picture to be taken. Considering that the period of interest of this study was set a few seconds between the event before the aircraft exit and the event after the parachute opening shock, what happened before or after this period is not considered. The barometric data provided approximate frames of where these events happened, as shown in Figure 2.

Figure 2. Barometric Pressure Sample

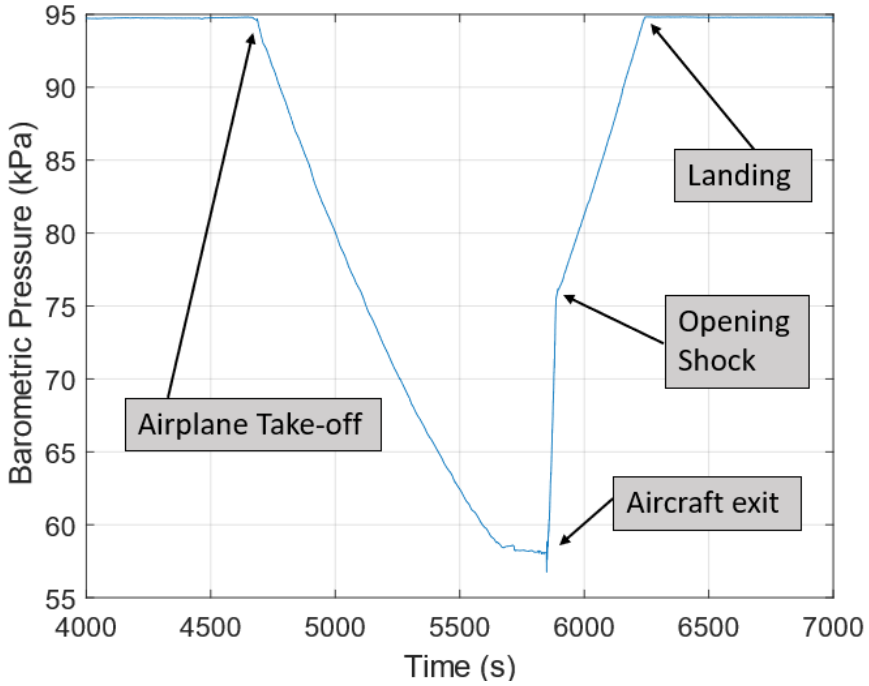

The trimmed data were stored as a .sto file compatible with OpenSim, and each sensor was mapped to skeletal bodies following the assignment shown in Table 2. The sensor assignment places the sensor at the body's center of mass and defines its orientation based on the quaternion rotation in space.

Table 2. Sensor Mapping

Sensor Name in .h5 file	Segment Name in Model
yel_HEAD	head_C1_imu
Chest	thoracic_region_imu
Belly	Abdomen_imu
RightUpperArm	humerus_r_imu
RightLowerArm	ulna_r_imu
LeftUpperArm	humerus_l_imu
LeftLowerArm	ulna_l_imu

The experimental data included information on the orientation of the sensor in the neutral posture, but it was not compatible with the musculoskeletal model. The problem arises from the experimental sensor orientation not being aligned with the global reference frame of the musculoskeletal model. However, with the pictures and knowing that all sensors had their local frame defined by the manufacturer, it was possible to define a calibration file with the sensors rotated to the desired orientation by a consecutive quaternion multiplication. A previous study inspired this approach, and its results were

checked by connecting the results to the inverse kinematics simulation (48). In summary, the procedure was to define the sensors' orientation, assign them to the bodies, run inverse kinematics, and observe the results to check how natural and physiologically accurate the motion was. This procedure required trial and error, but most of the used datasets had a similar sensor placement. In most cases, the same calibration file was valid, or the rotation of one or two sensors fixed the problem. In Figure 3, the model has a global reference frame, but each sensor is represented by a small yellow box with its local frame.

Figure 3. Musculoskeletal Model and Sensors Reference Frames

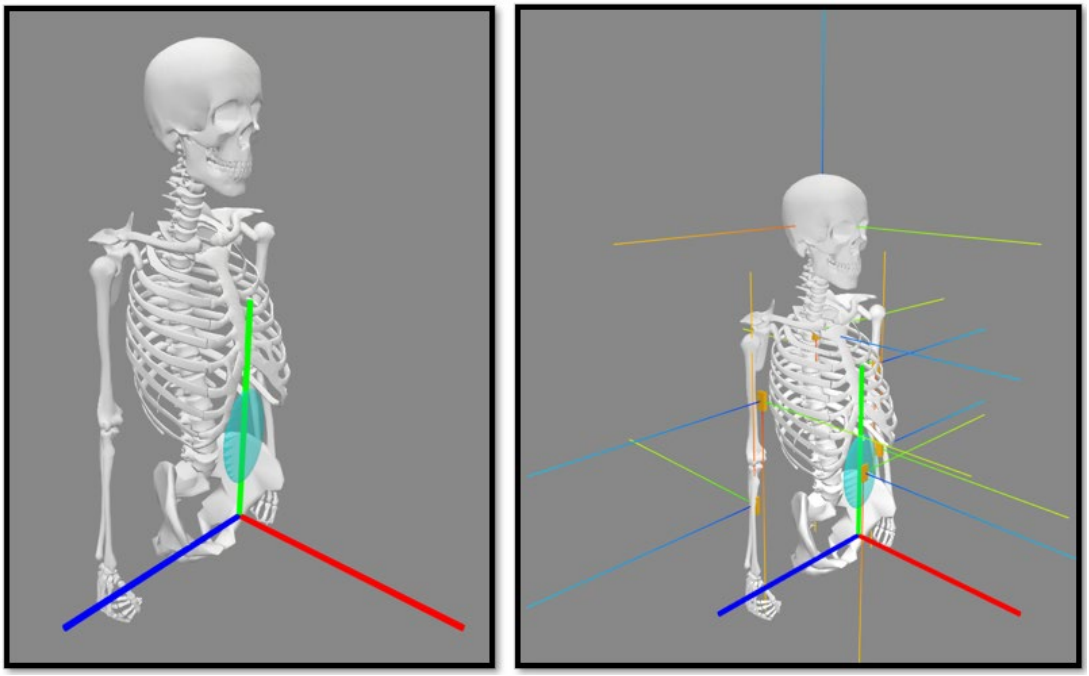

(a) Global Frame (b) Local Frame

INVERSE KINEMATICS AND DYNAMICS

The proposed methodology started with the modeling scaling (if necessary) and the IMU placement for calibration. Simultaneous with the model calibration, an initial inverse kinematics analysis was done to observe the musculoskeletal model motion and check its validity in the period of interest. The results from the musculoskeletal model animation provided a better estimate of the instant when the jumper leaves the aircraft and when the parachute is opened. The free-fall period observed was between 30 seconds and a minute for the HALO jumps, and for the HAHO jump, it was less than 10 seconds. Depending on the results of this step, the calibration was corrected or updated to have a final calibrated musculoskeletal model to run the final inverse kinematics simulation and obtain the joint angle profiles and body kinematics. Once the body kinematics were calculated, the results were combined with the estimated loads of the

risers and tether forces to calculate joint torques with the inverse dynamics tool. External forces were added to the model to analyze the effect of the tether snatch produced by the carried bundle and the opening shock produced by opening the parachute. The definition of external forces requires the location of the forces on the global reference frame and their magnitude as a function of time. Point loads were assumed for all the forces applied in the center of mass of the selected bodies. The bundle force was applied vertically down the abdominal wall.

In contrast, the parachute force is divided in half and applied symmetrically to the left and right clavicles and vertically upwards (49,50). The jumper and the bundle are assumed to be rigid bodies, as represented in Figure 4a. Figure 4b is the free body diagram of the jumper accelerating downwards after the aircraft exit but before the parachute opening shock.

Figure 4. Parachute Free-Fall Representation: a) Jumper and Bundle, b) Free Body Diagram of Jumper

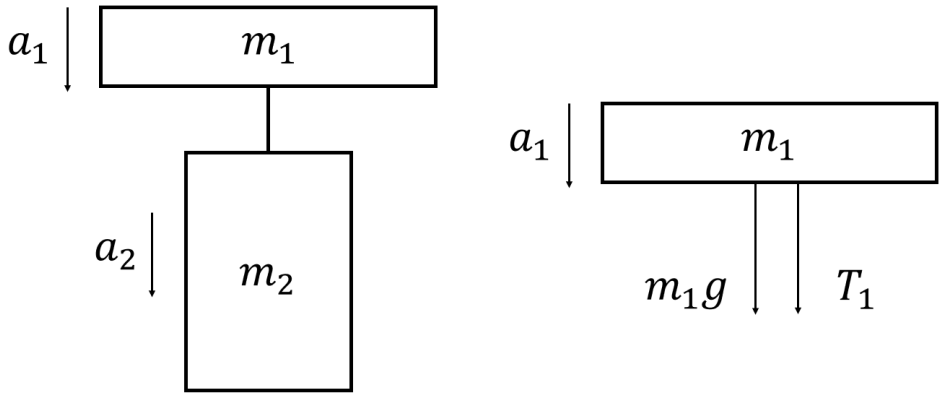

(a) (b)

The magnitude of the cable tension that connects the jumper and the bundle is obtained from the free-body diagram and by applying Newton's second law in the vertical direction. Air resistance is neglected, and the cable is assumed to be always in tension. The effects of air resistance are neglected since they are highly variable, and its calculation would require factors like air density, bundle cross-sectional area, and drag coefficient, which are outside the scope of this analysis and the available experimental data. The acceleration of the sensor attached to the abdominal wall is defined as the sum of the acceleration of the human body and gravity: $a_{s1} = a_1 + g$ where:

$$\sum F = m_1 a_1$$

$$m_1 g + T_1 = m_1 a_1$$

$$T_1 = m_1 a_{s1} - 2m_1 g$$

$$T_1 = m_1 (a_{s1} - 2g)$$

Figure 5: Free Body Diagram for Opening Shock

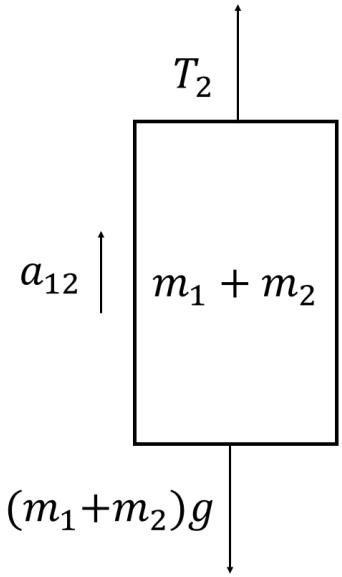

A similar analysis was done after the parachute opening shock, as shown in

Figure ***5***. In this case, it is assumed that the jumper and the bundle reach an equilibrium state, falling at a constant speed before the parachute opens. This assumption implies that the air drag causes a deceleration equal to the gravitational acceleration. Therefore, the force of the parachute is applied to one body with the combined masses. In this case, the data from the sensor placed over the chest is defined as: $a_{s2} = a_{12} + g$ where:

$$\sum F = (m_1 + m_2) a_{12}$$

$$T_2 - (m_1 + m_2) g = (m_1 + m_2) a_{12}$$

$$T_2 = (m_1 + m_2)(a_{s2} + g - g)$$

$$T_2 = (m_1 + m_2) a_{s2}$$

Since a_{s1} and a_{s2} change in time, the cable tension is also a function of time. Figure 6 shows the accelerometer readings from the “Belly” and “Chest” sensors that represent

a_{s1} and a_{s2}. The figure represents applying a linear envelope to the raw accelerometer data. The envelopes are determined using spline interpolation over local maxima separated by 250 samples.

Figure 6. Sample Accelerometer Information

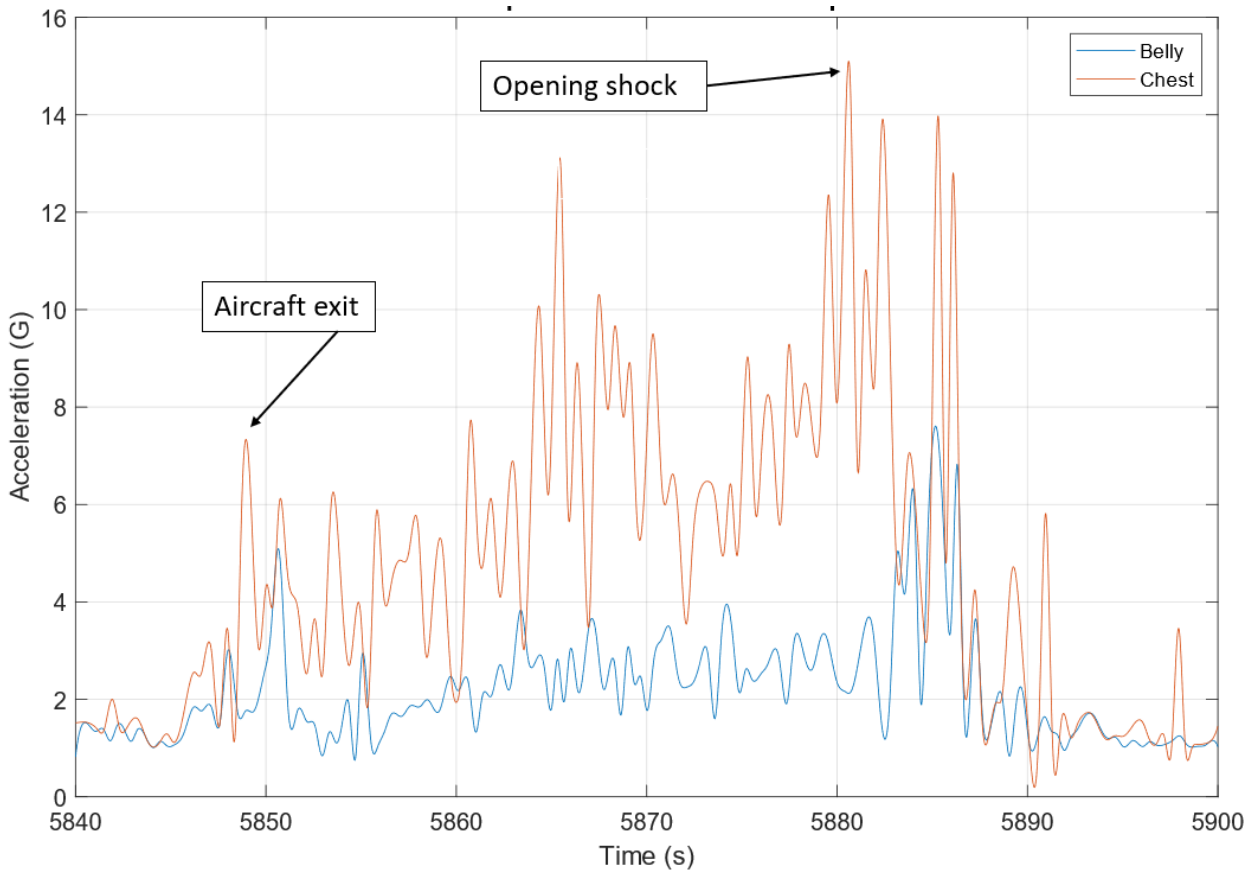

For the case of the shoulder model, it was impossible to run inverse kinematics with the IMU tool since the model was only compatible with the 3.3 version of OpenSim, and the IMU tools were included in the 4.0 versions and forward. The inverse kinematics results corresponding to the upper body model were remapped to the shoulder model global reference frame coordinates. Once the inverse kinematics simulations were completed, the procedure for inverse dynamics described previously in this section was followed. The only difference was that the bundle weight was applied to the sternum since the shoulder model does not have a defined abdominal wall body.

STATIC OPTIMIZATION

Muscle forces and activations were estimated using the static optimization tool in OpenSim. The necessary information to run the static optimization is the same as that

used for the inverse dynamics tool. In terms of results, the inverse dynamics simulation calculates generalized forces for translational joints and moments for rotational joints, while the static optimization simulation obtains muscle activation. The static optimization process is more computationally demanding for two reasons: the search process of the optimization and the fact that there are many more muscles than joints. Therefore, shorter simulations were run during the periods of interest instead of running just one simulation. The simulations were five seconds long each, and two or three simulations were done around the instant of the tether snatch and the parachute opening shock, respectively. The same procedure was followed for the upper body and shoulder models.

RESULTS

INVERSE KINEMATICS AND DYNAMICS

The inverse kinematics simulations result in joint angle profiles for all the degrees of freedom of the multiple body joints defined in the musculoskeletal model. From the 33 degrees of freedom defined in the DACAA model, the following results will concentrate on the neck and right shoulder joints. From Figure 7 to Figure 10, the joint angle profiles of the neck joint are presented; from Figure 11 to Figure 14, the right shoulder angular displacement are presented.

Figure 7. Neck Joint Angle Profiles from Purple Dataset

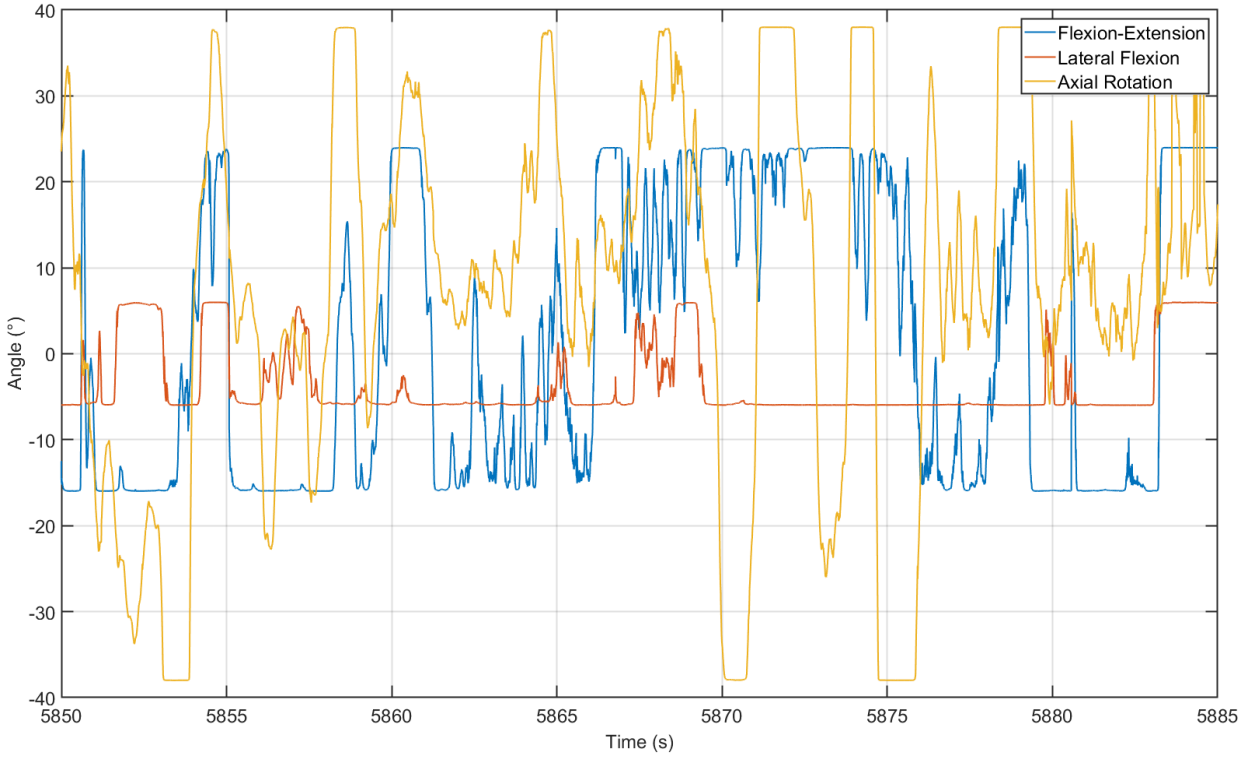

Figure 8. Neck Joint Angle Profiles from Yellow Dataset

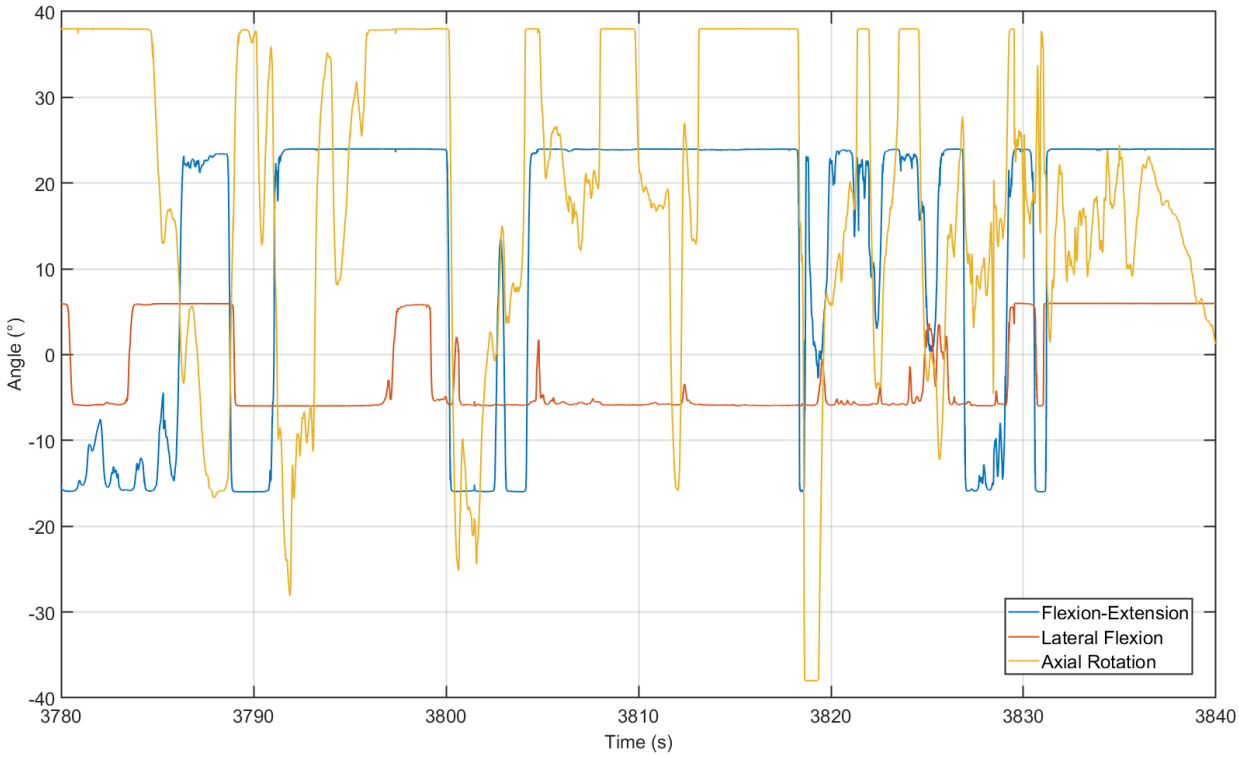

Figure 9. Neck Joint Angle Profiles from New Yellow Dataset

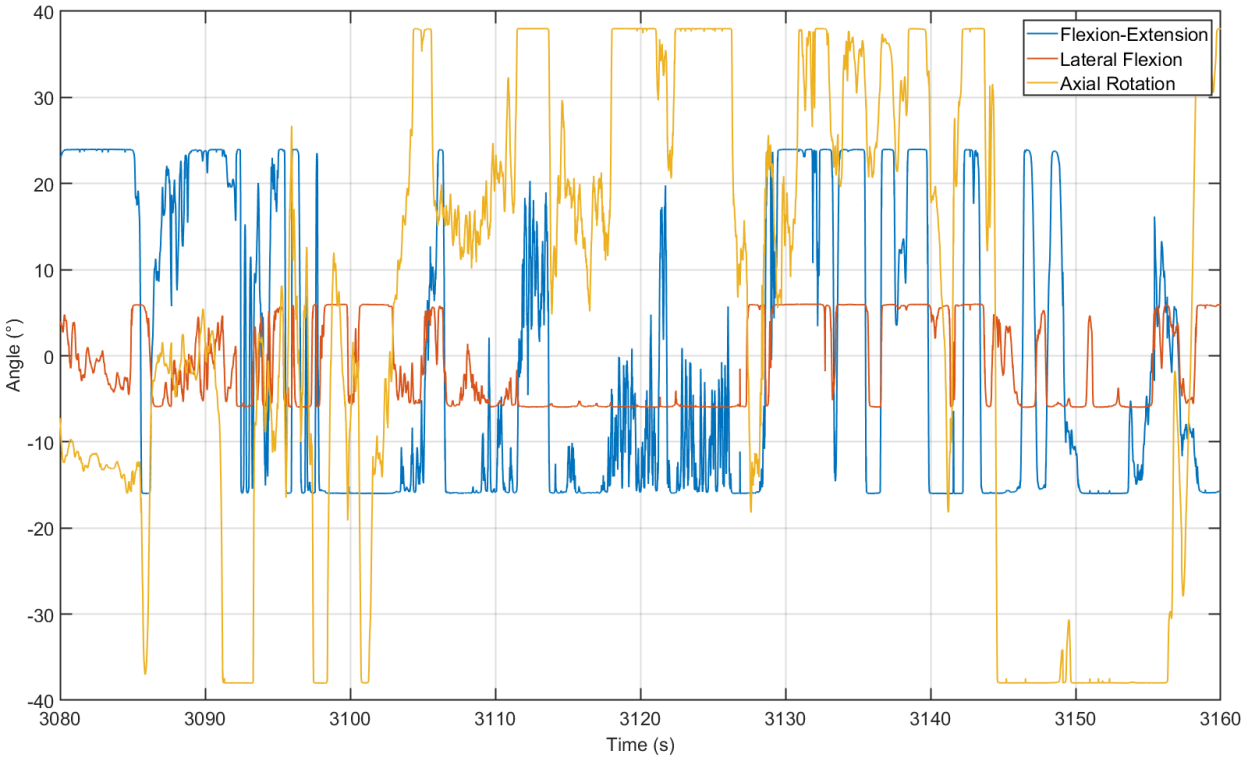

Figure 10. Neck Joint Angle Profiles from Red Dataset

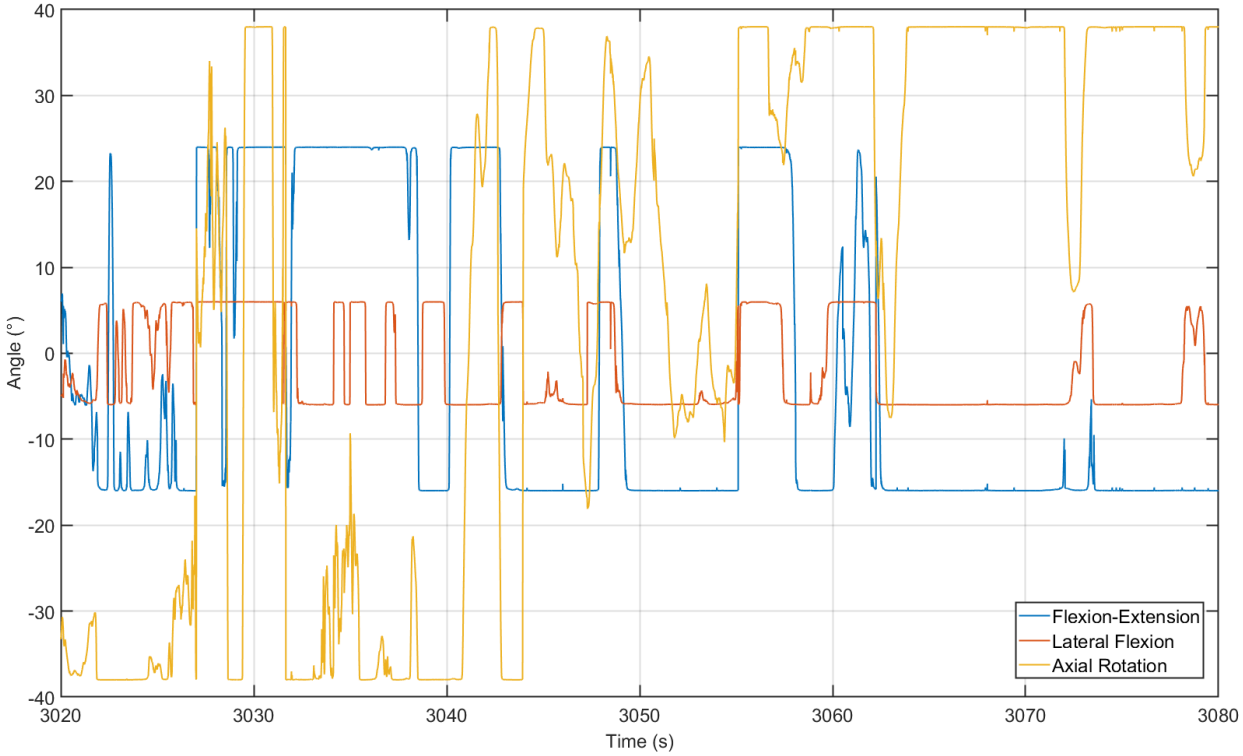

Figure 11. Right Shoulder Joint Angle Profiles from Purple Dataset

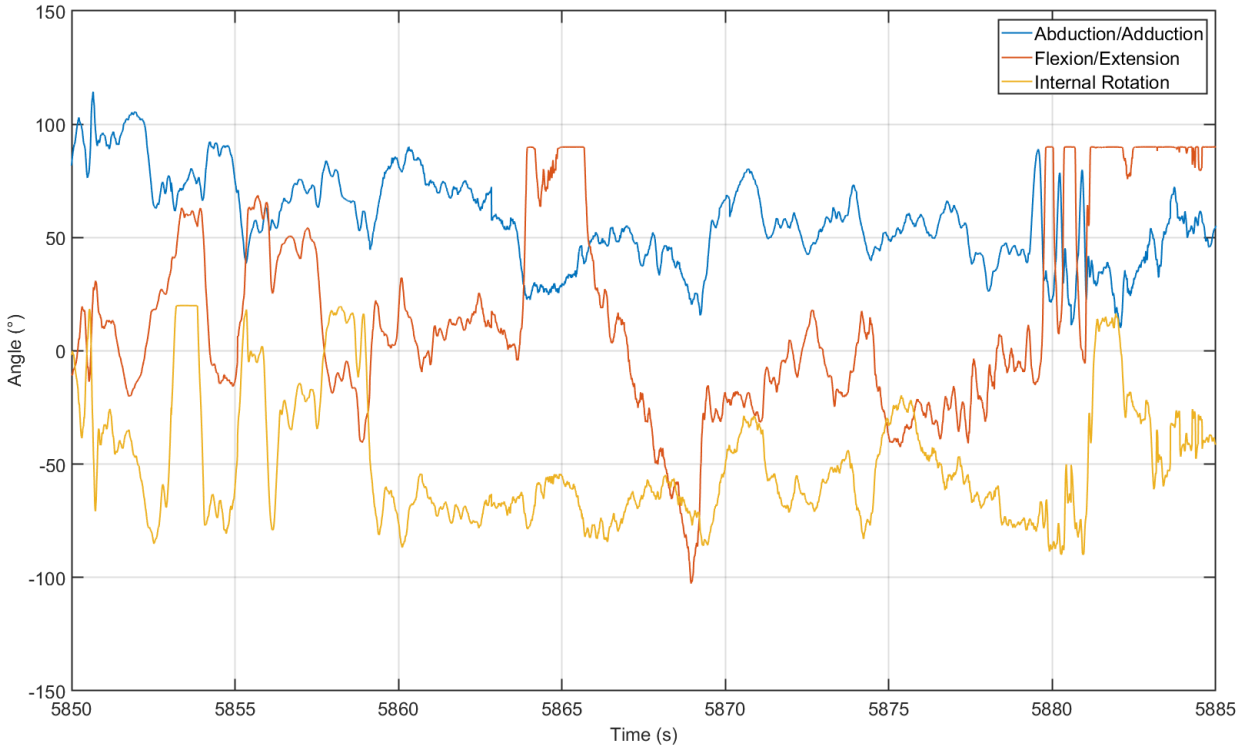

Figure 12. Right Shoulder Joint Angle Profiles from Yellow Dataset

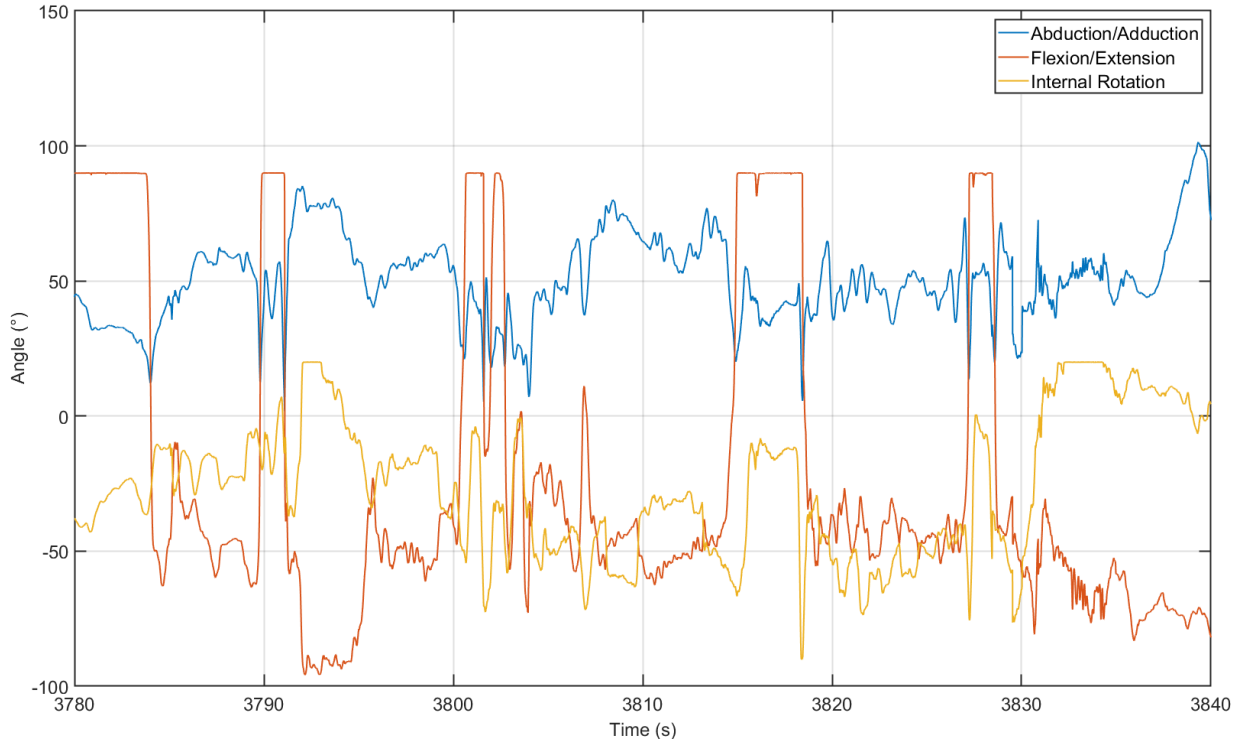

Figure 13. Right Shoulder Joint Angle Profiles from New Yellow Dataset

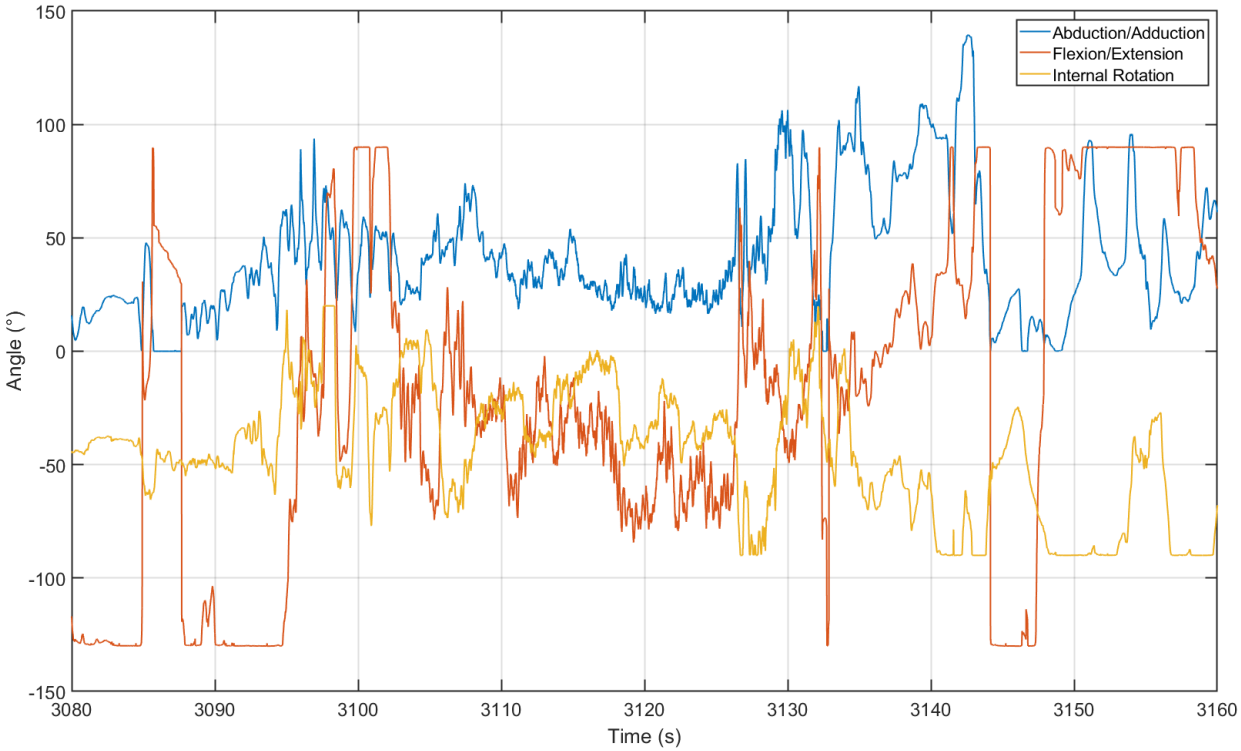

Figure 14. Right Shoulder Joint Angle Profiles from Red Dataset

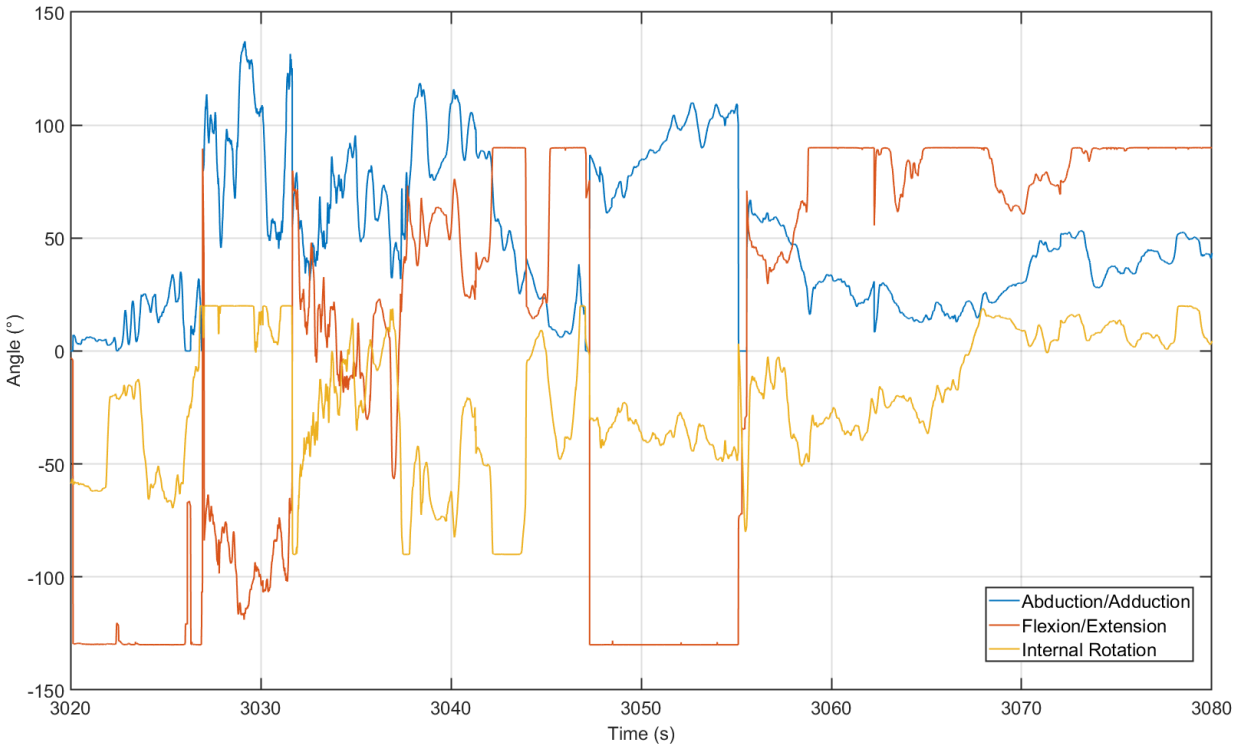

The joint angle profiles drive an OpenSim animation of the musculoskeletal model moving in space. As explained, checking the animation resulting from inverse kinematics is a simultaneous step during the sensor calibration part of the consecutive methodology steps to test the sensor orientation and placement. The animation identifies the period of interest and the key instants when the jumper leaves the aircraft and when the parachute is opened. The key moments during the animation correspond to the jumper inside the aircraft, a frame during free-fall, and another frame after the parachute opening. The snapshots for one of the datasets are shown in Figure 15 for the upper-body model and Figure 16 for the shoulder model. The figures also included the external forces as green arrows, the inputs for inverse dynamics, to ease the visualization of the parachute and bundle forces. The snapshots for the other datasets can be found in Appendix A.

Figure 15. Upper Body Model Animation Snapshots for Purple Dataset

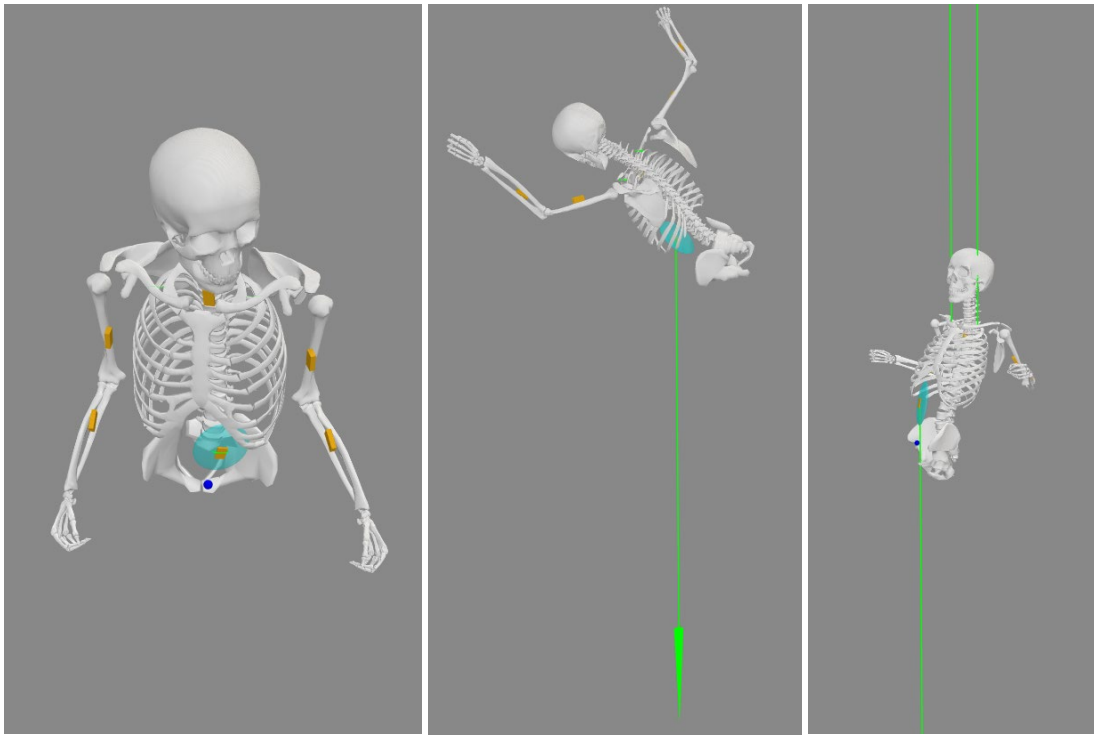

(a) Inside the Aircraft (b) Free-Fall (c) After Parachute Opening

Figure 16. Shoulder Model Animation Snapshots for Purple Dataset

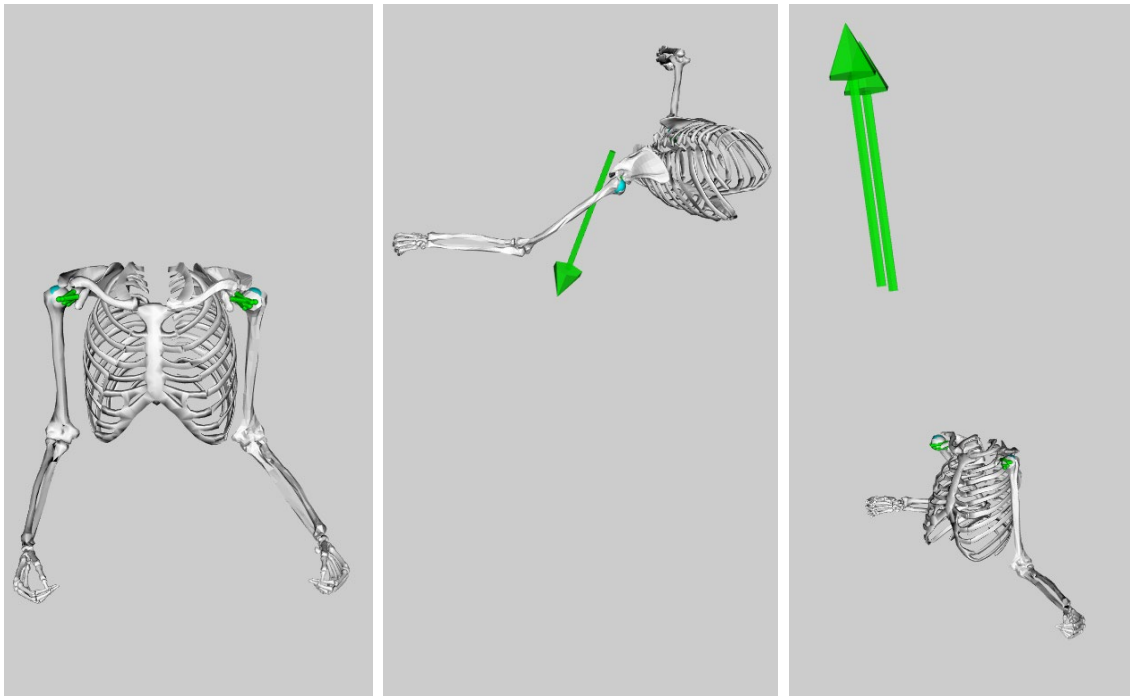

(a) Inside the Aircraft (b) Free-Fall (c) After Parachute Opening

Even when the force magnitude is the same for the upper body and the shoulder models, the point of view differs due to the OpenSim software release used for each one. The visualization tool differs in how it scales the green arrows representing the force. Small misalignments in the visualization of the same postures in the two models are caused by the global reference frame of the upper body, located at the pelvis's base, while the shoulder model is in the upper part of the sternum. The inverse dynamics simulations estimate the internal joint torques that produce motion. The neck joint rotational moments resulting from the inverse dynamics simulations are presented from Figure 17 to Figure 20.

Figure 17. Neck Joint Torque Profile for Purple Dataset

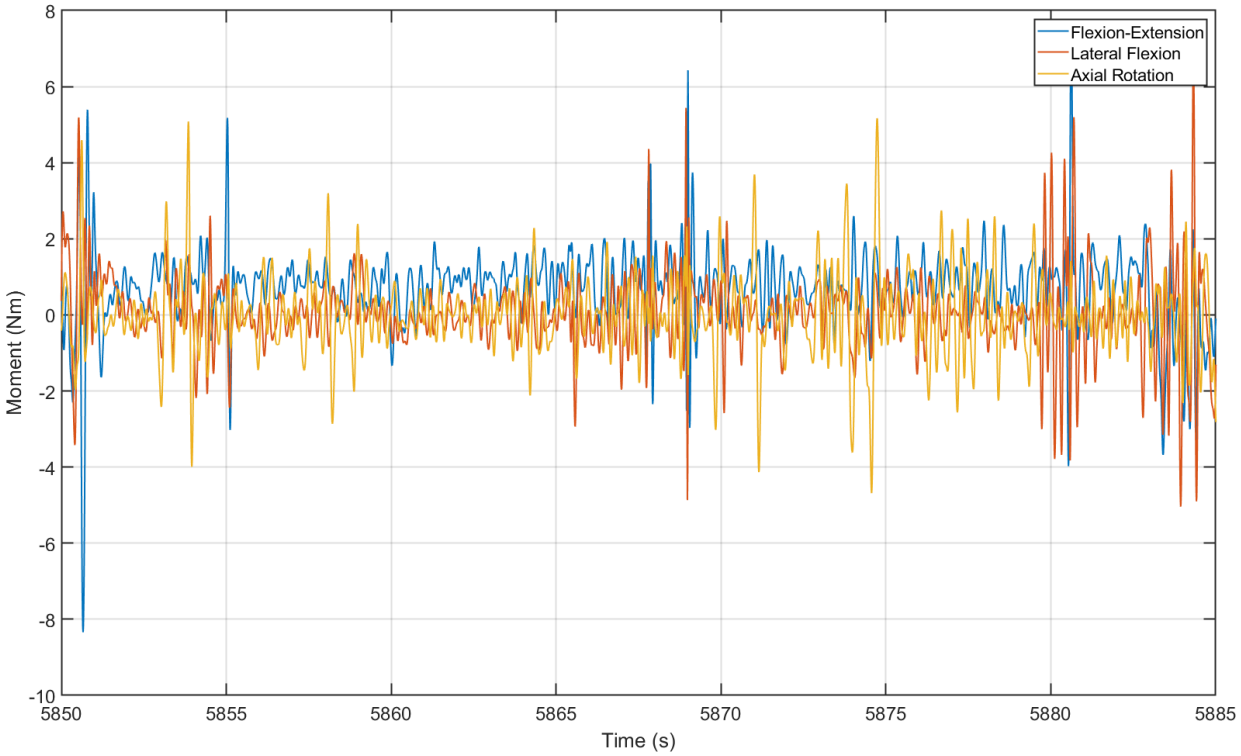

Figure 18. Neck Joint Torque Profile for Yellow Dataset

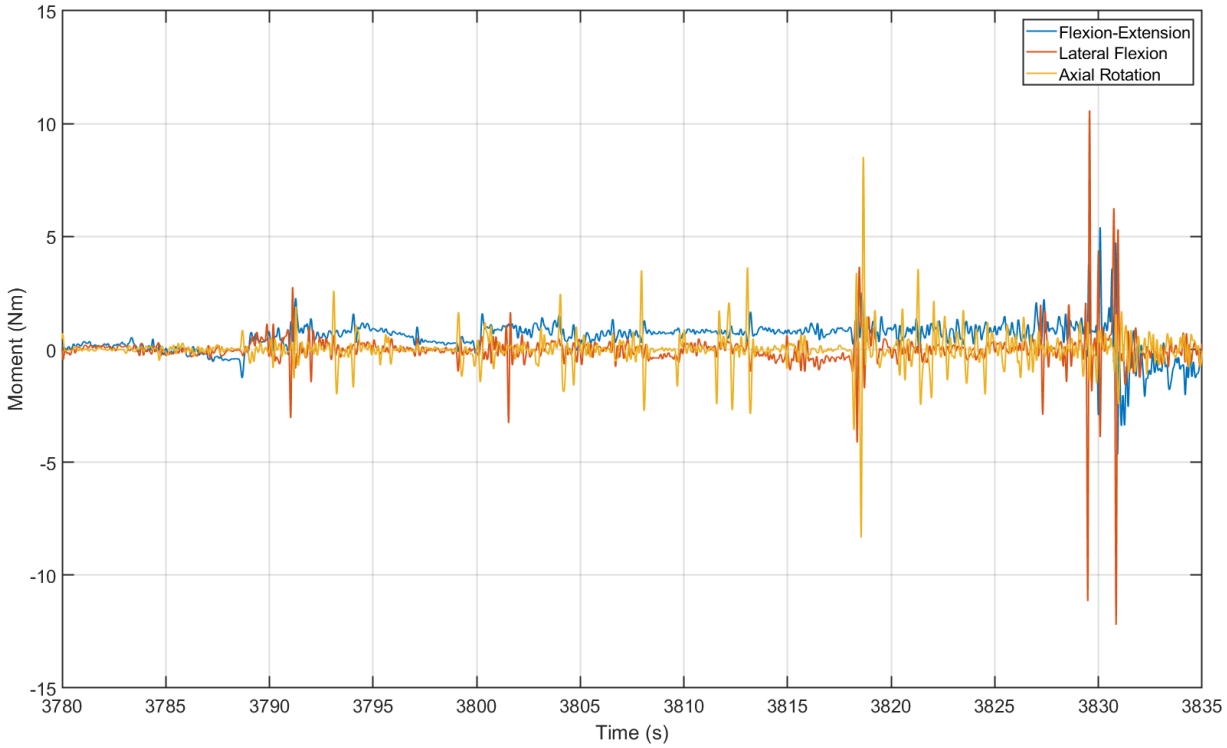

Figure 19. Neck Joint Torque Profile for New Yellow Dataset

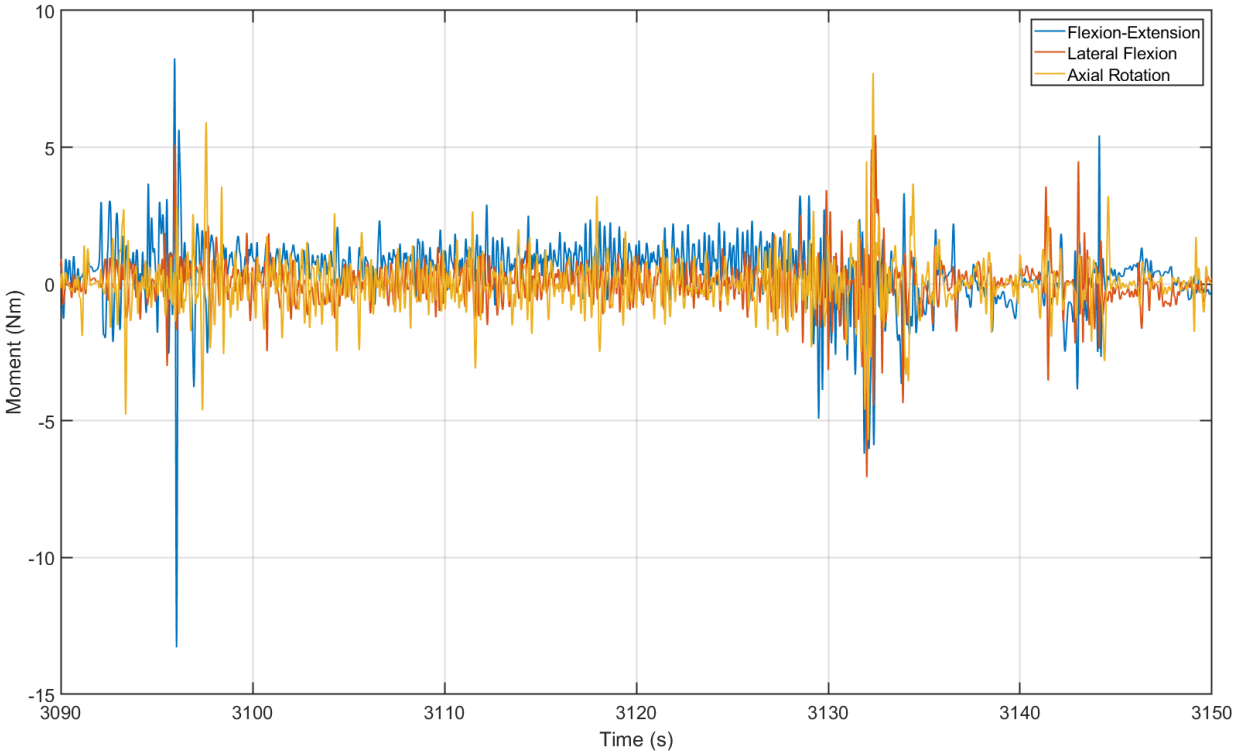

Figure 20. Neck Joint Torque Profile for Red Dataset

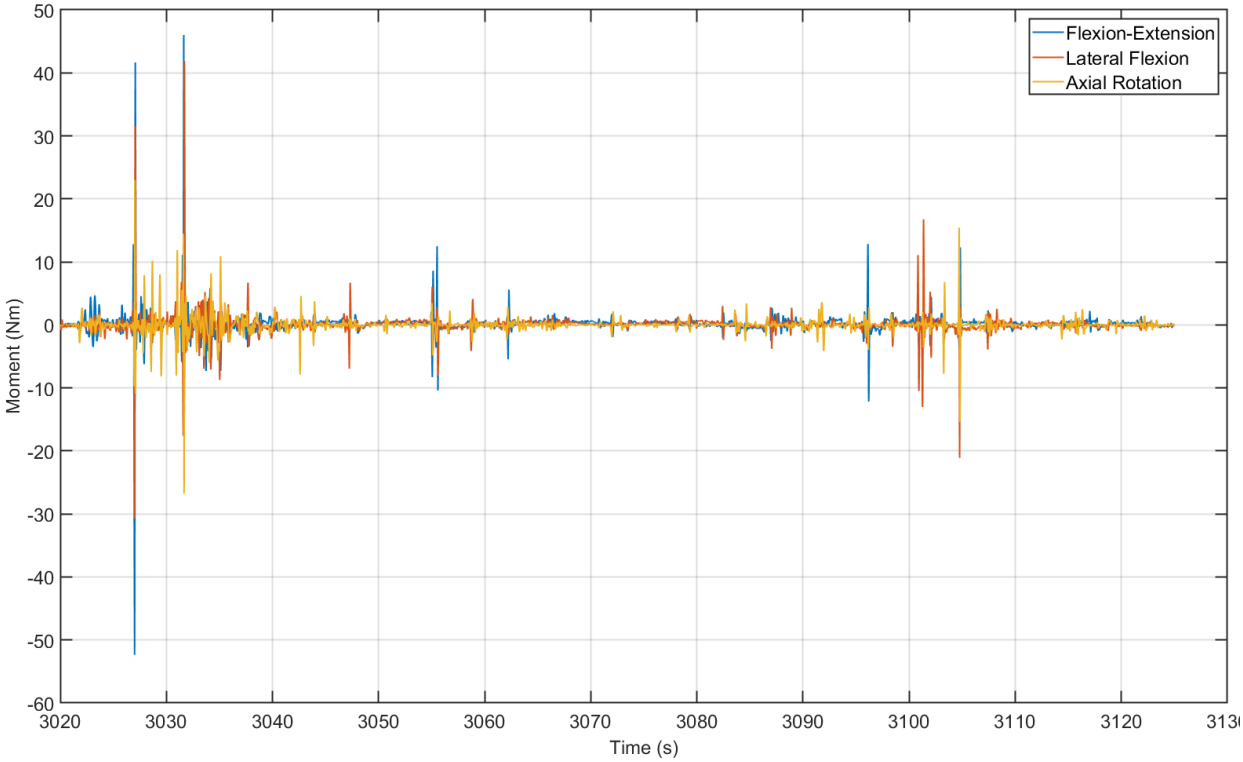

As observed for the neck joint torque profiles, there are some key instants where the joint torque reaches its peak value. In the case of the shoulder joint, the data has been summarized as a table instead of plots. The peak rotational moments for the different degrees of freedom of the shoulder joint are shown in Table 3. The magnitude of the rotational moments corresponds to the peak joint torque on a period defined from two seconds before the opening shock and two seconds after that.

Table 3. Maximum Shoulder Joint Torque During Parachute Opening

	Purple	Yellow	New Yellow	Red
Flexion (Nm)	264.68	124.77	155.84	2220.70
Extension (Nm)	242.71	174.48	137.08	1914.70
Abduction (Nm)	131.75	93.93	127.52	294.80
Adduction (Nm)	234.19	130.98	242.48	1713.60
Internal Rotation (Nm)	5.12	5.21	7.35	45.10
External Rotation (Nm)	19.54	4.91	13.64	70.50

STATIC OPTIMIZATION/SHOULDER JOINT ANALYSIS

In the case of static optimization, there are muscle activation and force data for each muscle defined in the model. As explained, simulations were run for five seconds of task time during the aircraft exit and parachute opening shock. Similar or the same frames from the animation were selected to show how the muscles are activated in the same postures shown in the previous sections. Muscle force and activation as a function of time can be observed in the output files from static optimization for the 394 muscles in the upper body model and the 100 muscles from the shoulder model. The muscle activation in the musculoskeletal model can be seen in Figure 21 for the upper body model and Figure 22 for the shoulder model. The visual representation of muscle activation for the remaining datasets can be found in Appendix B.

Figure 21. Upper Body Model Muscle Activation for Purple Dataset

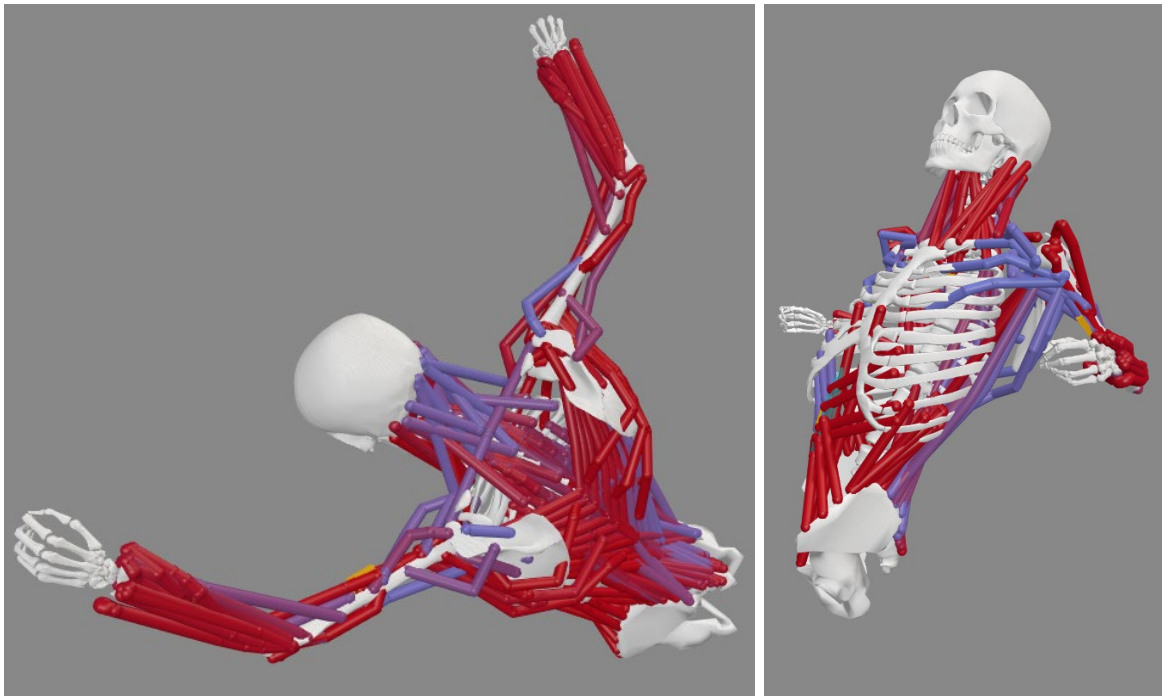

(a) Free Fall (b) After Parachute Opening

Figure 22. Shoulder Model Muscle Activation for Purple Dataset

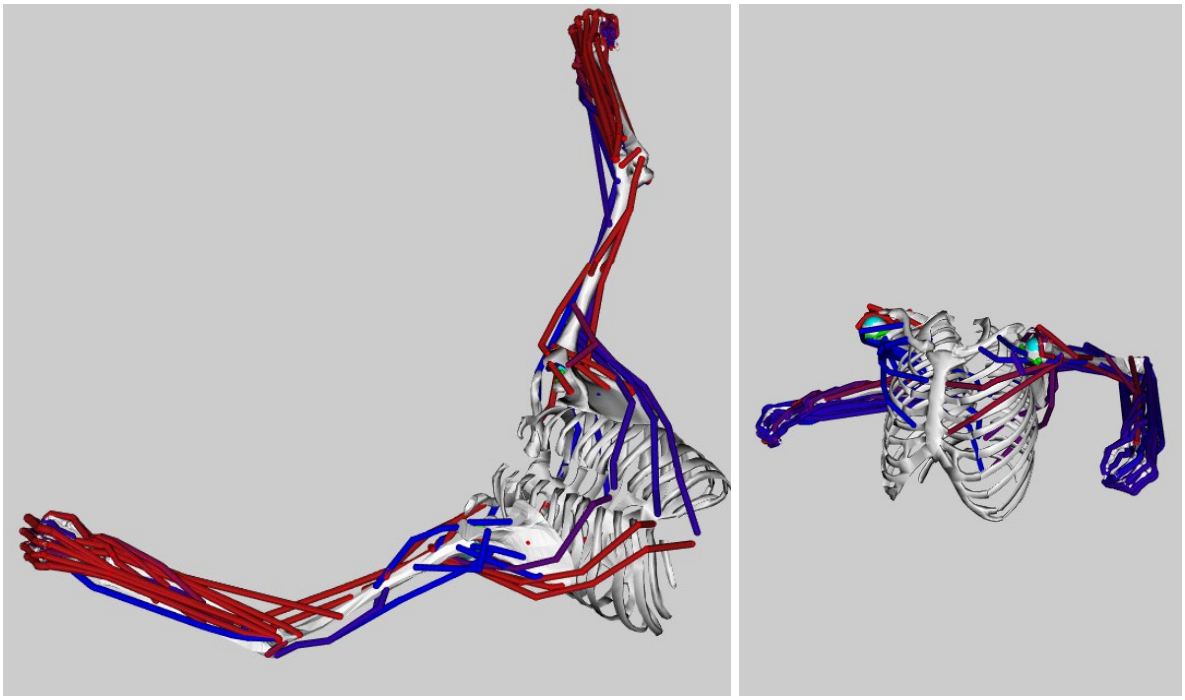

(a) Free-Fall (b) After Parachute Opening

DISCUSSION

METHODOLOGY CHOSEN AND DEVELOPED

The study presented in the current report uses a standard methodology in OpenSim for musculoskeletal modeling that follows consecutive steps of musculoskeletal scaling and calibration, inverse kinematics, inverse dynamics, and static optimization. The OpenSim simulations resulted in joint angle profiles, internal moment, and muscle activation.

The necessary data to start the simulation and complete the described steps are obtained through a sensor-based motion capture setup with IMU sensors. The sensor rotation in space feeds the inverse kinematics step to obtain body segment orientations as a function of time. In the case of inverse dynamics, in addition to the kinematics results, external loading must be defined to obtain body joint torques. The literature describes multiple methods to apply external loadings to musculoskeletal models (51). The cited methods have their advantages and disadvantages regarding complexity and computation time. The external loading magnitude and development rate are estimated using the accelerometer data from the IMUs.

Having pre- and post-jumping calibration trial recordings with corresponding pictures in multiple planes (sagittal, frontal, and coronal) would eliminate the necessity of trial-and-error processes to place the IMU sensors in the musculoskeletal model. Knowing the orientation of the sensor could directly create a valid calibration file for any case. Because sensors shift, move, or even fall off, documenting those changes improves the simulation and modeling results' robustness. Increasing the number of sensors could also be beneficial. Besides the chest and abdomen IMUs, pelvis and shoulder sensors could result in a more detailed spine motion. This approach also includes the possibility of adding sensors for the lower limb, making a full-body musculoskeletal body analysis possible. Reducing the sampling rate could be beneficial in storage and computational power requirements to process the data. Nevertheless, the methodology described in the report provides a valuable starting point for more detailed analyses. Future work is required to confirm that down sampling procedure did not affect the proposed analysis results, but at the present time, it is believed that this procedure did not compromise the analysis.

INVERSE KINEMATICS AND DYNAMICS

The results from the inverse kinematics simulation are joint angle profiles where maximum displacement in each direction can be obtained. Even when the results show the angular displacement of every joint, the joint definition in the musculoskeletal model prevents all joints from moving out of the safe range of motion. During the simulation, even when the sensor data could cause a body segment motion outside the safe range of motion, the inverse kinematics algorithm guards against that. It can be observed from Figure 7 to Figure 14 that the flexion/extension and axial rotation angle profiles have a horizontal trend in some periods, meaning that the algorithm prevented going above or below the joint angle limits. Preventing hyperextension allows the model animation to be more natural. Considering that all the following steps of the methodology process rely on the results from inverse kinematics, it is crucial to guarantee the human-like motion of the musculoskeletal model. The angular displacement of body joints can be understood as the result of an internal moment developed due to muscle activation. The inverse dynamics simulation aims to calculate the necessary torques to produce the motion defined by the inverse kinematics results. The inverse dynamics simulation uses the model motion and external forces as inputs. The current report presents a methodology where the accelerometer data is processed with a linear envelope to obtain the peak moments in the periods of interest. Other filtering and smoothing techniques could be tested to see how the peak of the joint torques changes. Most recent processing testing has shown promising results with a moving average approach.

In the same way, as for joint angles, there are limits to the amount of internal torque that a joint can produce. Experimentally, the joint strength can be measured for its multiple degrees of freedom, which can be interpreted as the limits for the dynamic joint strength. Multiple studies have measured joint strength for the neck joint in isometric and isokinetic

testing. Most studies concentrate on flexion-extension and lateral bending movements (52) or compare healthy and non-healthy groups (53). Table 4 summarizes results from two studies (85) on rugby players (85) and adults in various age groups (54). The neck joint moments shown from Figure 17 to Figure 20 correspond to the peak internal loading moment during the opening shock and the tether snatch, while the referenced studies report joint strength (produced by muscle activation) produced in different directions. With this information, volunteers undergoing strength training, similar to what U.S. Army personnel do, values below the peak torque have been reported in the literature. In the case of the Red dataset, loading conditions go above that limit but in the same order of magnitude. The high loading observed for the Red dataset (Figure 20 and Table 3) could be explained by the small time frame between the aircraft exit and the parachute opening. The lack of enough time to reach a mid-air equilibrium state causes the body to experience rapid changes in the experienced acceleration.

Table 4. Peak Neck Strength

	Flexion (Nm)	Extension (Nm)	Right Lateral Bending (Nm)	Left Lateral Bending (Nm)
Olivier & Du Toit, 2008	38.93	56.19	59.69	58.92
Olivier et al., 2010	29.53	48.35	48.41	48.84

The current musculoskeletal models have anatomical limits for the allowable range of motion, so even when the sensor information could drive the model in a certain way, the joint limits do not allow the inverse kinematics simulation to result in those displacements. On the other hand, there are no limits to the joint torques the inverse dynamic simulations could output, s limitations when trying to relate the simulation results with the allowable torques a joint can develop with a certain motion. Future work could dive into potential OpenSim model modifications to improve the proposed methodology.

STATIC OPTIMIZATION

OpenSim software has multiple alternatives to estimate muscle force and activation. Previous researchers have investigated the differences between static optimization and computed muscle control, suggesting that static optimization is a better approach (55,56). Running computed muscle control was tested as part of this study, but it required extra steps that would not result in a better methodology for this project. Even when specific muscles were not considered when analyzing the muscle activation results, it is important to analyze the body's behavior under those loading conditions. If maximal voluntary contraction (MVC) could be obtained for each jumper, their muscle activation could provide a deeper understanding of how the jumper moves mid-air to open the parachute and a greater understanding on the impact on the body after the opening shock.

As for future work, the current results from inverse kinematics, inverse dynamics, and static optimization could be used as boundary conditions to run finite element model simulations. Full-body models or specific regions, like cervical and lumbar spines, can be loaded with rotational moments or angular displacements. The finite element model simulations would provide insights into how stress is distributed in bones and soft tissue (57,58). Additionally, by knowing the force produced by the muscle activation, the results from static optimization could be used as boundary conditions to run finite element models. A previous study has mapped the muscle insertion points to simulate the lumbar spine during a sit-to-stand task (59). Regardless, these proposed future studies, while providing more insight on the impact on the jumper, the necessary groundwork in the methodology to be employed was developed and described in this report.

CONCLUSIONS

- A new methodology was developed to understand the biomechanical analysis of parachute opening shock by utilizing advanced technologies such as IMUs and validated musculoskeletal models.

- The magnitude of the joint torques observed for the HAHO jump could be caused by the fast change from being inside the aircraft to free-fall and experiencing the opening shock.
- For both HALO and HAHO jumps, increasing the carried weight also increases the magnitude of the combined loading the body experiences.

- The complexities of parachute jumping-related injuries involve multifaceted factors, demanding a holistic and multidisciplinary approach for a comprehensive understanding and consecutive injury assessment.

RECOMMENDATIONS

- Including more sensors during data collection, especially around the back, could result in a more precise animation of the musculoskeletal model.

- More complex alternatives for external loading definitions could be explored to improve the results of the inverse dynamic since the parachute riser and bundle forces are distributed over the jumper harness.

- The static optimization results could be validated with muscle activation measurements by including surface electromyography sensors in the experimental protocol.

- Joint strength measurement can be collected from each jumper, so there would be a more direct comparison with the results from inverse dynamics simulations regarding the torque a particular joint can produce.

- Simulations with multiple jumpers to ensure generalizability of the present results are valid across jumpers.

REFERENCES

1. Farrow GB. Military static line parachute injuries. Australian and New Zealand Journal of Surgery. 1992 Mar 21;62(3):209–14.
2. Knapik J, Steelman R. Risk factors for injuries during military static line airborne operations: A systematic review and meta-analysis. J Athl Train. 2016 Nov 1;51(11):962–80.
3. Maneechaeye W, Deepreecha K, Jiamjarasrangsi W. Incidence and risk factors associated with injuries during static line parachute training in Royal Thai Army. Mil Med Res. 2020 Dec 7;7(1):27.
4. Ekeland A. Injuries in military parachuting: a prospective study of 4499 jumps. Injury. 1997 Apr;28(3):219–22.
5. Gruppo L, Mader TH, Wedmore I. Ocular problems in military free fall parachutists. Mil Med. 2002 Oct 1;167(10):797–800.
6. Glorioso JE, Batts KB, Ward WS. Military free fall training injuries. Mil Med. 1999 Jul;164(7):526–30.
7. Department of the Army. Special Forces Military Free-Fall Operations (FM 3-05.211). Washington, DC: Department of the Army: Headquarters; 2005.
8. Gong X, Han L, Wang J, Ran M. Recognition and simulation of parachute action based on continuous hidden Markov model. In: 2017 Chinese Automation Congress (CAC) [Internet]. IEEE; 2017. p. 4108–13. Available from: http://ieeexplore.ieee.org/document/8243500/
9. Mokhtarzadeh H, Yeow CH, Hong Goh JC, Oetomo D, Malekipour F, Lee PVS. Contributions of the soleus and gastrocnemius muscles to the anterior cruciate ligament loading during single-leg landing. J Biomech. 2013 Jul;46(11):1913–20.
10. Kar J, Quesada PM. A musculoskeletal modeling approach for estimating anterior cruciate ligament strains and knee anterior–posterior shear forces in stop-jumps performed by young recreational female athletes. Ann Biomed Eng. 2013 Feb 27;41(2):338–48.
11. Baek SY, Ajdaroski M, Shahshahani PM, Beaulieu ML, Esquivel AO, Ashton-Miller JA. A comparison of inertial measurement unit and motion capture measurements of tibiofemoral kinematics during simulated pivot landings. Sensors. 2022 Jun 11;22(12):4433.
12. Ciklacandir S, Ozkan S, Isler Y. A Comparison of the performances of video-based and IMU sensor-based motion capture systems on joint angles. In: 2022 Innovations in Intelligent Systems and Applications Conference (ASYU). IEEE; 2022. p. 1–5.

13. Delgado-García G, Vanrenterghem J, Ruiz-Malagón EJ, Molina-García P, Courel-Ibáñez J, Soto-Hermoso VM. IMU gyroscopes are a valid alternative to 3D optical motion capture system for angular kinematics analysis in tennis. Proc Inst Mech Eng P J Sport Eng Technol. 2021 Mar 21;235(1):3–12.

14. Lee CJ, Lee JK. Inertial motion capture-based wearable systems for estimation of joint kinetics: A systematic review. Sensors. 2022 Mar 25;22(7):2507.

15. Jang S, Park S bog, Moon S bog, Kim JM, Lee S uk. Comparison of camera based and Inertial measurement unit based motion analysis. In: Proceedings of the 7th International Conference on Sensor Networks. SCITEPRESS - Science and Technology Publications; 2018. p. 161–7.

16. Freire S, Santos G, Armondes A, Meneses EAL, Wanderley MM. Evaluation of inertial sensor data by a comparison with optical motion capture data of guitar strumming gestures. Sensors. 2020 Oct 8;20(19):5722.

17. Miranda-Oliveira P, Branco M, Fernandes O. Accuracy and Interpretation of the acceleration from an inertial measurement unit when applied to the sprint performance of track and field athletes. Sensors. 2023 Feb 4;23(4):1761.

18. de Ruiter CJ, Wilmes E, Brouwers SAJ, Jagers EC, van Dieën JH. Concurrent validity of an easy-to-use inertial measurement unit-system to evaluate sagittal plane segment kinematics during overground sprinting at different speeds. Sports Biomech. 2022 Mar 30;1–14.

19. Punchihewa NG, Miyazaki S, Chosa E, Yamako G. Efficacy of inertial measurement units in the evaluation of trunk and hand kinematics in baseball hitting. Sensors. 2020 Dec 20;20(24):7331.

20. Nijmeijer EM, Heuvelmans P, Bolt R, Gokeler A, Otten E, Benjaminse A. Concurrent validation of the Xsens IMU system of lower-body kinematics in jump-landing and change-of-direction tasks. J Biomech. 2023 Jun;154:111637.

21. Hafer JF, Mihy JA, Hunt A, Zernicke RF, Johnson RT. Lower extremity inverse kinematics results differ between inertial measurement unit- and marker-derived gait data. J Appl Biomech. 2023 Jun 1;39(3):133–42.

22. Chiaverini S, Siciliano B. The Unit Quaternion: A useful tool for inverse kinematics of robot manipulators. Syst Anal Model Simul. 1999 Jan;35(1):45–60.

23. Gladh K, Äng BO, Lindholm P, Nilsson J, Westman A. Decelerations and muscle responses during parachute opening shock. Aviat Space Environ Med. 2013 Nov 1;84(11):1205–10.

24. Rooks TF, Novotny BL, McGovern SM, Winegar A, Shivers BL, Brozoski FT. Evaluation of head and body kinematics experienced during parachute opening shock. Mil Med. 2021 Nov 2;186(11–12):e1149–56.

25. Lo Martire R, Gladh K, Westman A, Lindholm P, Nilsson J, Äng BO. Neck muscle activity in skydivers during parachute opening shock. Scand J Med Sci Sports [Internet]. 2016 Mar;26(3):307–16. Available from: https://onlinelibrary.wiley.com/doi/10.1111/sms.12428

26. Sibson BE, Banks JJ, Yawar A, Yegian AK, Anderson DE, Lieberman DE. Using inertial measurement units to estimate spine joint kinematics and kinetics during walking and running. Sci Rep. 2024 Jan 2;14(1):234.

27. Gladh K, Lo Martire R, Äng BO, Lindholm P, Nilsson J, Westman A. Decelerations of parachute opening shock in skydivers. Aerosp Med Hum Perform [Internet]. 2017 Feb 1;88(2):121–7. Available from: http://www.ingentaconnect.com/content/10.3357/AMHP.4731.2017

28. Wolf D. A Simplified dynamic model of parachute inflation. J Aircr. 1974 Jan;11(1):28–33.

29. Wolf D. Parachute opening shock. In: 15th Aerodynamic Decelerator Systems Technology Conference. Reston, Virginia: American Institute of Aeronautics and Astronautics; 1999.

30. Wehrly D. Low Altitude, High Speed Personnel Parachuting: Medical and Physiological Issues. US Army Aeromedical Research Laboratory. 1987 Feb 1;87(3).

31. Doherr K. Extended parachute opening shock estimation method. In: 17th AIAA Aerodynamic Decelerator Systems Technology Conference and Seminar. Reston, Virginia: American Institute of Aeronautics and Astronautics; 2003.

32. Lee C. Experimental investigation of full-scale and model parachute opening. In: 8th Aerodynamic Decelerator and Balloon Technology Conference. Reston, Virginia: American Institute of Aeronautics and Astronautics; 1984.

33. Sahin T, Batın S. A descriptive study of orthopedic injuries due to parachute jumping in soldiers. BMC Emerg Med. 2020 Dec 31;20(1):58.

34. Dhar D. Retrospective study of injuries in military parachuting. Med J Armed Forces India. 2007 Oct;63(4):353–5.

35. Donisi L, Cesarelli G, Coccia A, Panigazzi M, Capodaglio EM, D'Addio G. Work-related risk assessment according to the revised NIOSH lifting equation: A preliminary study using a wearable inertial sensor and machine learning. Sensors. 2021 Apr 7;21(8):2593.

36. McEntire B, Alem N, Brozoski F. McEntire, B., Alem, N., & Brozoski, F. (2004). Parachutist neck injury risk associated with head-borne weight. US Army Med Dep J. 2004;30(4).

37. Nilsson J, Fridén C, Burén V, Westman A, Lindholm P, Äng BO. Musculoskeletal pain and related risks in skydivers: A population-based survey. Aviat Space Environ Med. 2013 Oct 1;84(10):1034–40.

38. Seth A, Hicks JL, Uchida TK, Habib A, Dembia CL, Dunne JJ, et al. OpenSim: Simulating musculoskeletal dynamics and neuromuscular control to study human and animal movement. Schneidman D, editor. PLoS Comput Biol [Internet]. 2018 Jul 26;14(7):e1006223. Available from: https://dx.plos.org/10.1371/journal.pcbi.1006223

39. Delp SL, Anderson FC, Arnold AS, Loan P, Habib A, John CT, et al. OpenSim: Open-source software to create and analyze dynamic simulations of movement. IEEE Trans Biomed Eng [Internet]. 2007 Nov;54(11):1940–50. Available from: http://ieeexplore.ieee.org/document/4352056/

40. Kucuk S, Bingul Z. The inverse kinematics solutions of industrial robot manipulators. In: Proceedings of the IEEE International Conference on Mechatronics, 2004 ICM ’04. IEEE; p. 274–9.

41. Kenwright B. Inverse kinematics with dual-quaternions, exponential-maps, and joint limits. Int J Adv in Intelligent Syst 2013 1(6): 53-65.

42. Cheng Z, Hu J, Yang J, Sanford DP, Hoyt RW, Zientara GP. Individualized avatars with complete anatomy: repositioning of superficial anatomy. US Army Research Institute of Environmental Medicine (USARIEM) Technical Reports T20-06. 2020.

43. Raabe ME, Chaudhari AMW. An investigation of jogging biomechanics using the full-body lumbar spine model: Model development and validation. J Biomech [Internet]. 2016 May;49(7):1238–43. Available from: https://linkinghub.elsevier.com/retrieve/pii/S0021929016302317

44. Cazzola D, Holsgrove TP, Preatoni E, Gill HS, Trewartha G. Cervical Spine injuries: A whole-body musculoskeletal model for the analysis of spinal loading. PLoS One. 2017 Jan 4;12(1):e0169329.

45. Saul KR, Hu X, Goehler CM, Vidt ME, Daly M, Velisar A, et al. Benchmarking of dynamic simulation predictions in two software platforms using an upper limb musculoskeletal model. Comput Methods Biomech Biomed Engin. 2015 Oct 3;18(13):1445–58.

46. Holzbaur KRS, Murray WM, Delp SL. A Model of the upper extremity for simulating musculoskeletal surgery and analyzing neuromuscular control. Ann Biomed Eng. 2005 Jun;33(6):829–40.

47. McFarland DC, McCain EM, Poppo MN, Saul KR. Spatial dependency of glenohumeral joint stability during dynamic unimanual and bimanual pushing and pulling. J Biomech Eng. 2019 May 1;141(5).

48. Mihy JA, Wagatsuma M, Cain SM, Hafer JF. Minimizing the effect of IMU misplacement with a functional orientation method. medRxiv [Internet]. 2022 Jan 1;2022.11.29.22282894. Available from: http://medrxiv.org/content/early/2022/11/29/2022.11.29.22282894.abstract

49. Baus J, Rooks TF, Tharion WJ, Hoyt R, French Krahn HA, Yang J. Inverse kinematics analysis based on parachute jumpers' inertial measurement units (IMUs) data. In: SAFE Association Symposium Proceedings. Virginia Beach, VA; 2023.

50. Baus J, Rooks TF, Tharion WJ, Hoyt R, French Krahn HA, Yang J. Musculoskeletal model-based neck generalized force estimation during parachute opening shock with and without a bundle. In: SAFE Association Symposium Proceedings. Virginia Beach, VA; 2023.

51. Akhavanfar M, Uchida TK, Clouthier AL, Graham RB. Sharing the load: modeling loads in OpenSim to simulate two-handed lifting. Multibody Syst Dyn. 2022 Feb 17;54(2):213–34.

52. Chavarro-Nieto C, Beaven M, Gill N, Hébert-Losier K. Neck strength in rugby union players: a systematic review of the literature. Phys Sportsmed. 2021 Oct 2;49(4):392–409.

53. Cagnie B, Cools A, De Loose V, Cambier D, Danneels L. Differences in isometric neck muscle strength between healthy controls and women with chronic neck pain: The use of a reliable measurement. Arch Phys Med Rehabil. 2007 Nov;88(11):1441–5.

54. Olivier P, du Toit E, du Randt R, Venter D. Isokinetic strength of the neck muscles. Isokinet Exerc Sci. 2010 Aug 13;18(3):169–77.

55. Lin YC, Dorn TW, Schache AG, Pandy MG. Comparison of different methods for estimating muscle forces in human movement. Proc Inst Mech Eng H. 2012 Feb 16;226(2):103–12.

56. Roelker SA, Caruthers EJ, Hall RK, Pelz NC, Chaudhari AMW, Siston RA. Effects of optimization technique on simulated muscle activations and forces. J Appl Biomech. 2020 Aug 1;36(4):259–78.

57. Tahmid S, Love BM, Liang Z, Yang J. Cervical spine finite element models for healthy subjects: development and validation. J Comput Inf Sci Eng. 2023 Aug 1;23(4).

58. Xu M, Yang J, Lieberman IH, Haddas R. Lumbar spine finite element model for healthy subjects: development and validation. Comput Methods Biomech Biomed Engin. 2017 Jan 2;20(1):1–15.

59. Honegger JD, Actis JA, Gates DH, Silverman AK, Munson AH, Petrella AJ. Development of a multiscale model of the human lumbar spine for investigation of tissue loads in people with and without a transtibial amputation during sit-to-stand. Biomech Model Mechanobiol. 2021 Feb 7;20(1):339–58.

APPENDIX A

Figure A1. Upper Body Model Animation Snapshots for Yellow Dataset: (a) Inside the Aircraft, (b) Free–Fall, (c) After Parachute Opening

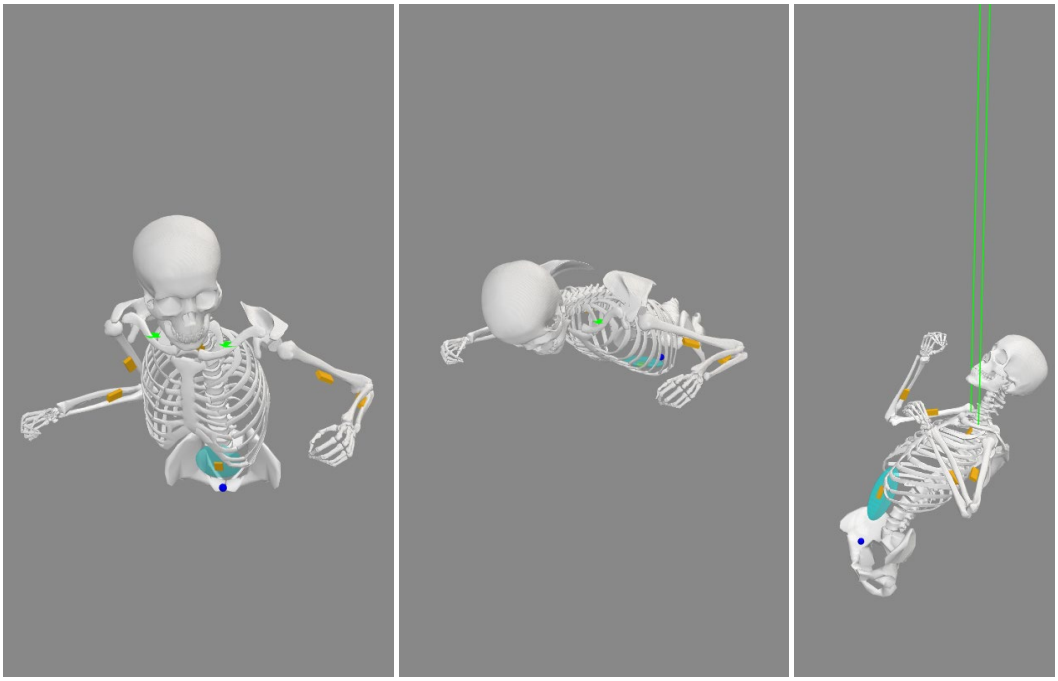

(a) (b) (c)

Figure A2. Upper Body Model Animation Snapshots for New Yellow Dataset: (a) Inside the Aircraft, (b) Free–Fall, (c) After Parachute Opening

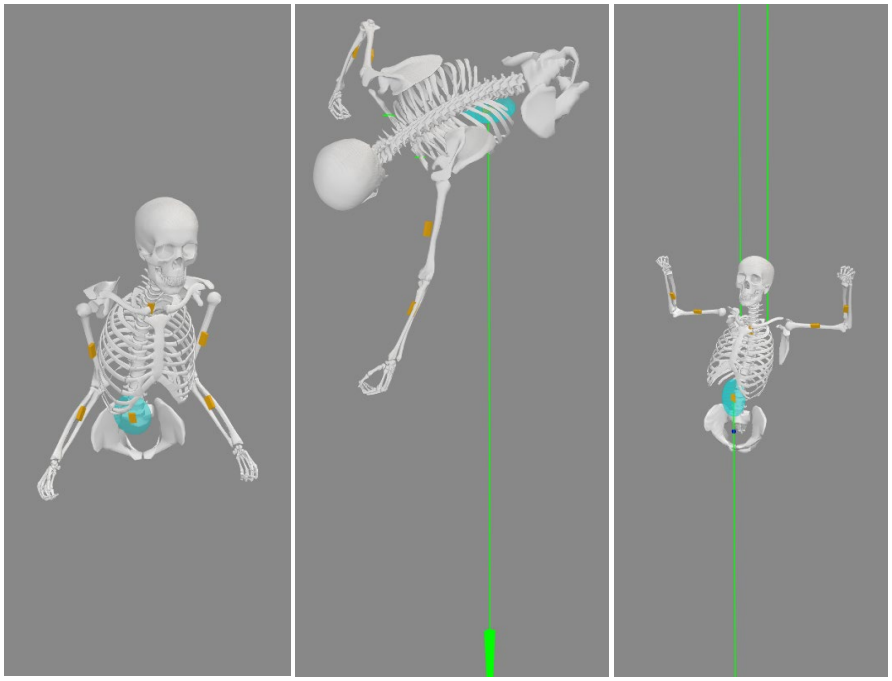

(a) (b) (c)

Figure A3. Upper Body Model Animation Snapshots for Red Dataset: (a) Inside the Aircraft, (b) Free–Fall, (c) After Parachute Opening

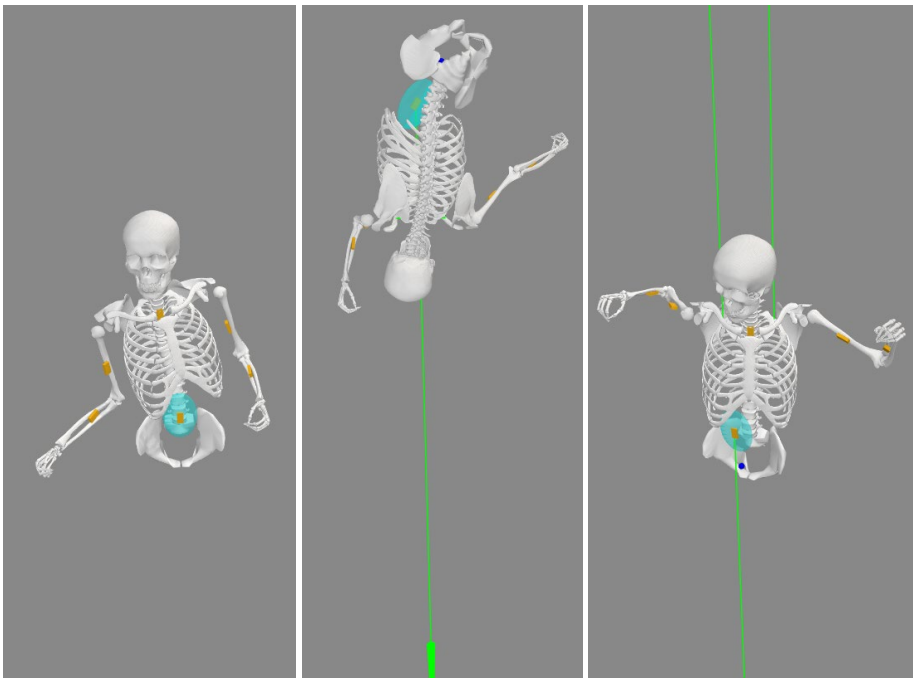

(a) (b) (c)

Figure A4. Shoulder Model Animation Snapshots for Yellow Dataset: (a) Inside the Aircraft, (b) Free–Fall, (c) After Parachute Opening

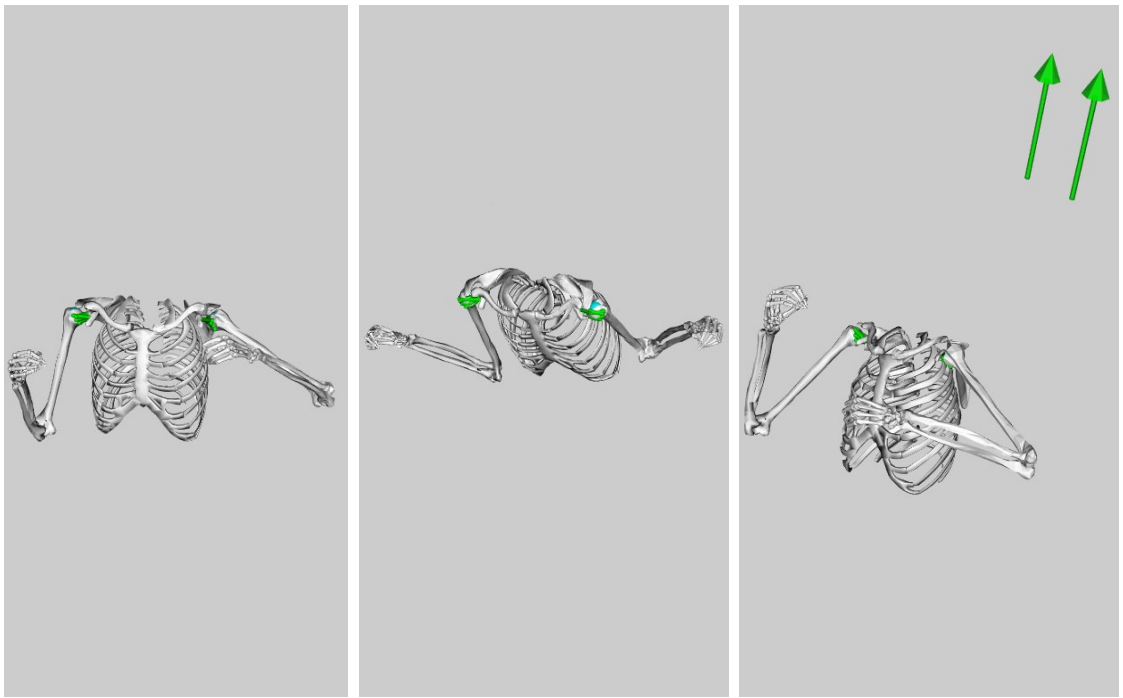

(a) (b) (c)

Figure A5. Shoulder Model Animation Snapshots for New Yellow Dataset: (a) Inside the Aircraft, (b) Free–Fall, (c) After Parachute Opening

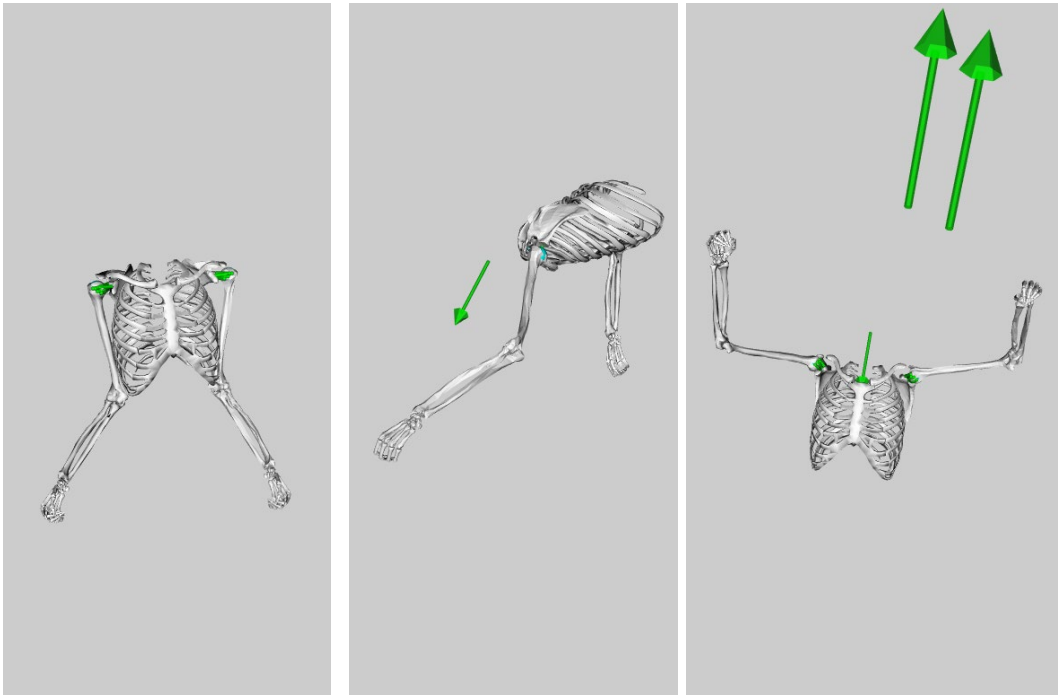

(a) (b) (c)

Figure A6. Shoulder Model Animation Snapshots for Red Dataset: (a) Inside the Aircraft, (b) Free–Fall, (c) After Parachute Opening

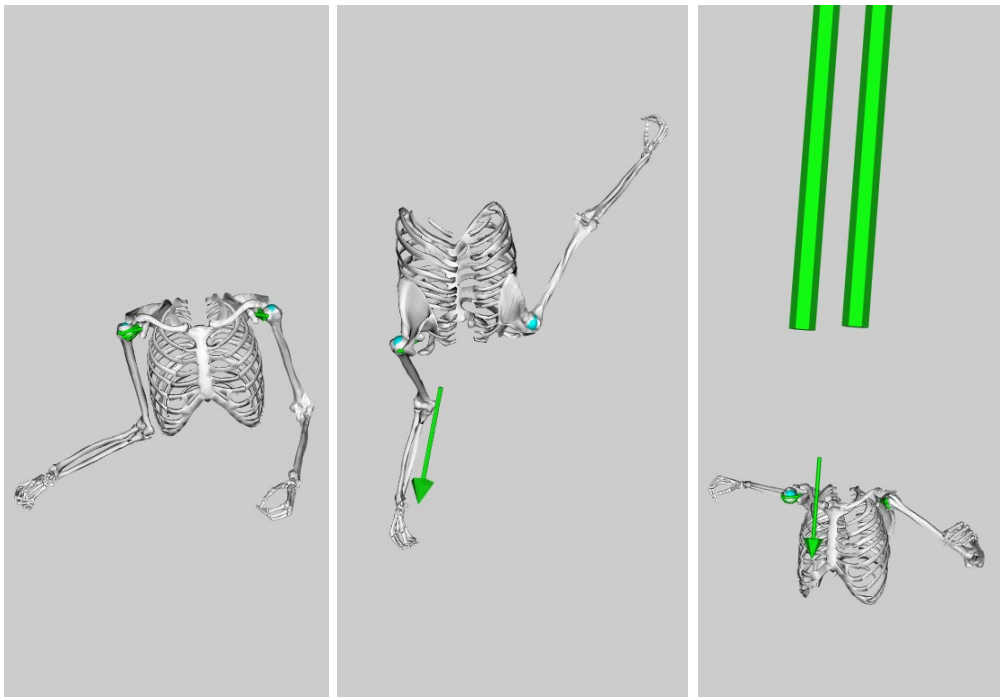

(a) (b) (c)

APPENDIX B

Figure B1. Upper Body Model Muscle Activation for Yellow Dataset: (a) Free–Fall, (b) After Parachute Opening

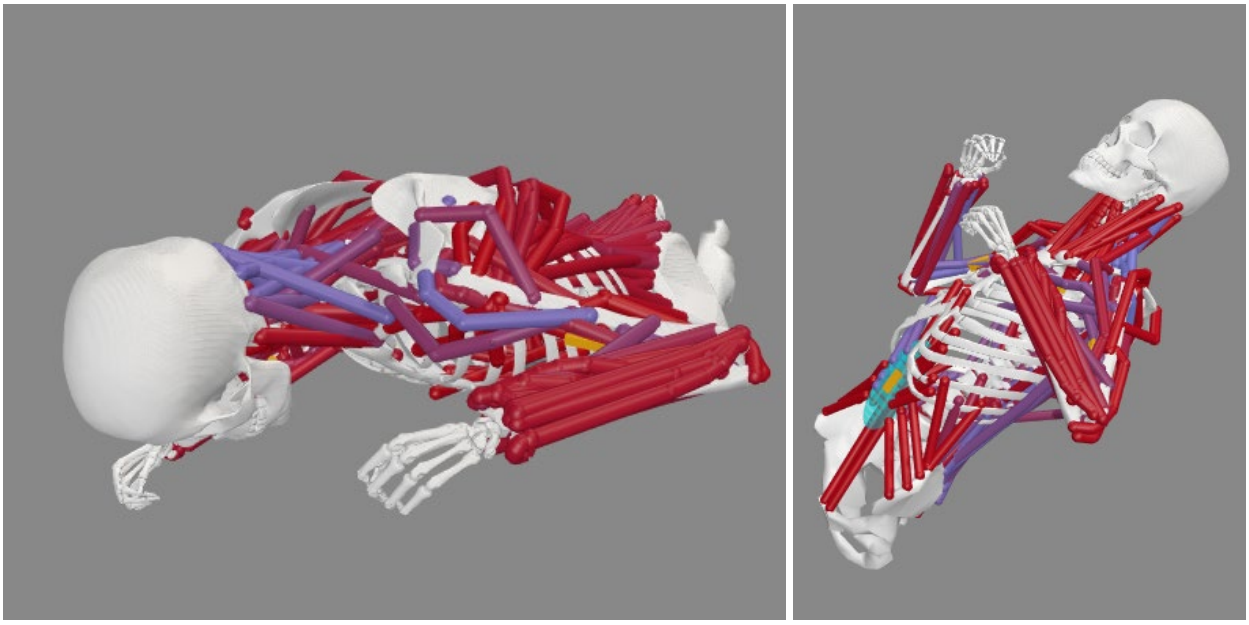

(a) (b)

Figure B2. Upper Body Model Muscle Activation for New Yellow Dataset: (a) Free–Fall, (b) After Parachute Opening

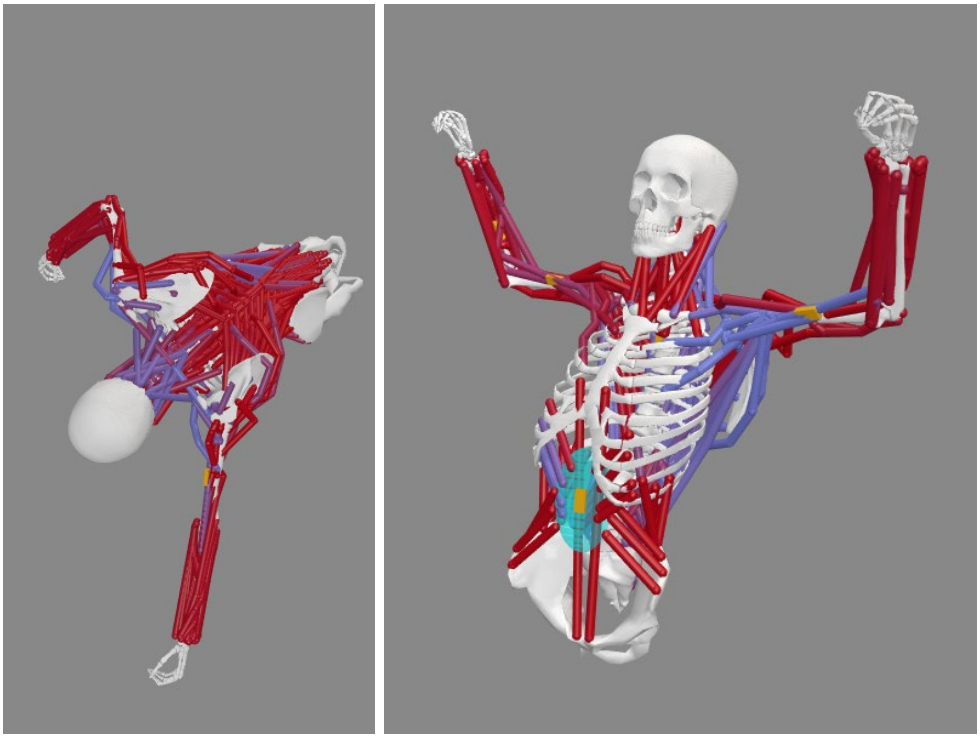

(a) (b)

Figure B3. Upper Body Model Muscle Activation for Red Dataset: (a) Free–Fall, (b) After Parachute Opening

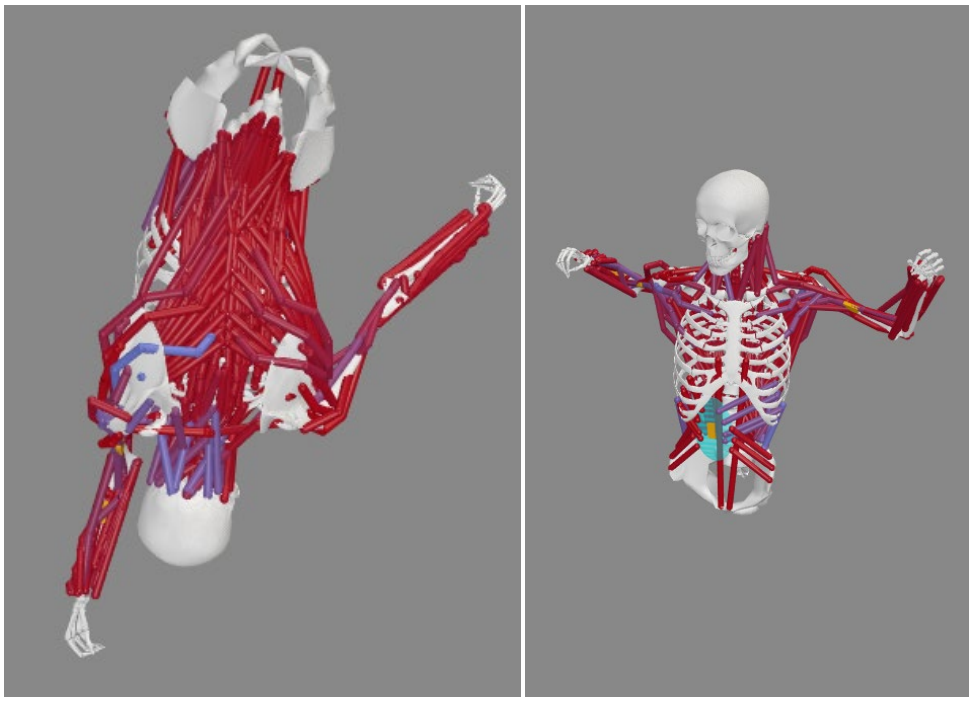

(a) (b)

Figure B4. Shoulder Model Muscle Activation for Yellow Dataset: (a) Free–Fall, (b) After Parachute Opening

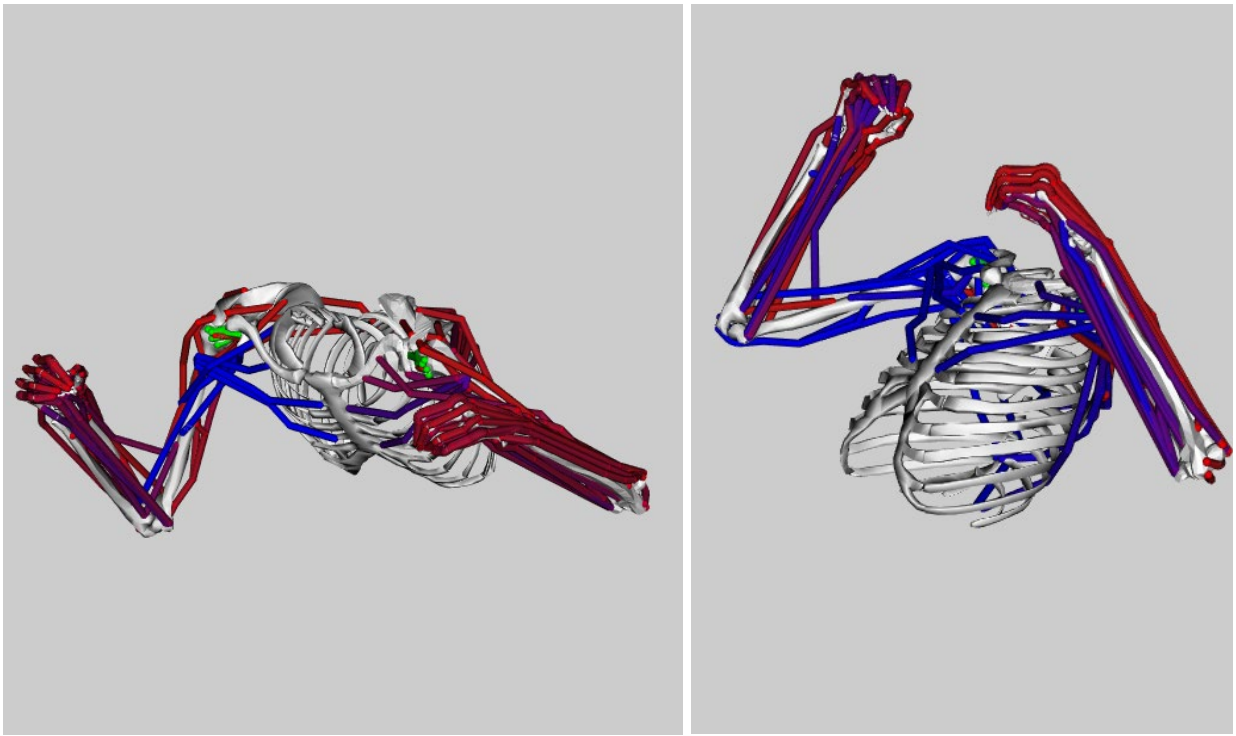

(a) (b)

Figure B5. Shoulder Model Muscle Activation for New Yellow Dataset: (a) Free–Fall, (b) After Parachute Opening

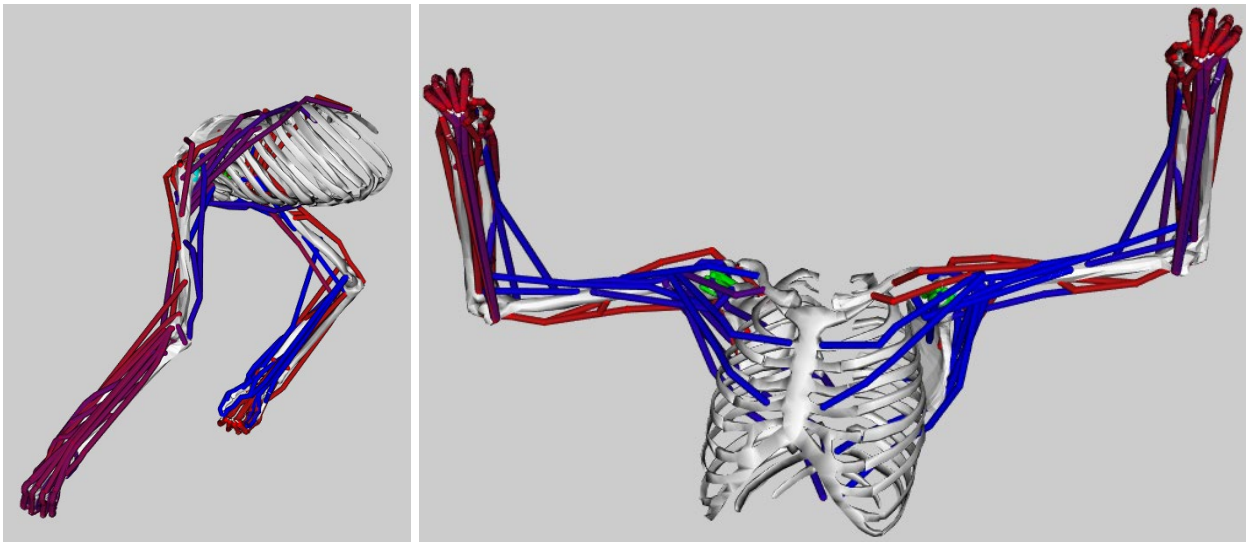

(a) (b)

Figure B6. Shoulder Model Muscle Activation for Red Dataset: (a) Free–Fall, (b) After Parachute Opening

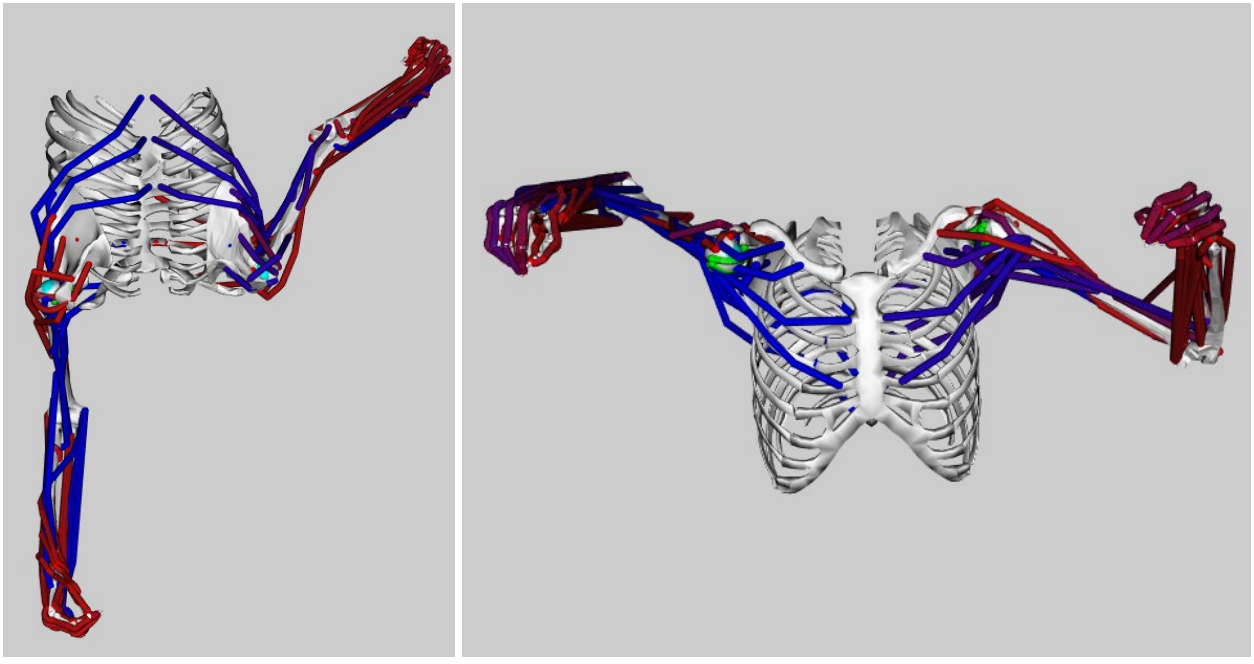

(a) (b)